Atypical epigenetic and small RNA control of degenerated transposons and their fragments in clonally reproducing *Spirodela polyrhiza*

Rodolphe Dombey, Daniel Buendía-Ávila, Verónica Barragán-Borrero, et al.

Genome Res. published online March 4, 2025
Access the most recent version at doi:10.1101/gr.279532.124

Atypical epigenetic and small RNA control of degenerated transposons and their fragments in clonally reproducing *Spirodela polyrhiza*

Rodolphe Dombey,[1,3] Daniel Buendía-Ávila,[1,2,3] Verónica Barragán-Borrero,[1] Laura Diezma-Navas,[1] Arturo Ponce-Mañe,[1] José Mario Vargas-Guerrero,[1,4] Rana Elias,[1] and Arturo Marí-Ordóñez[1]

[1]*Gregor Mendel Institute of Molecular Plant Biology (GMI) of the Austrian Academy of Sciences, Vienna 1030, Austria;* [2]*Vienna BioCenter PhD Program, Doctoral School of the University of Vienna and Medical University of Vienna, Vienna 1030, Austria*

A handful of model plants have provided insight into silencing of transposable elements (TEs) through RNA-directed DNA methylation (RdDM). Guided by 24 nt long small-interfering RNAs (siRNAs), this epigenetic regulation installs DNA methylation and histone modifications like H3K9me2, which can be subsequently maintained independently of siRNAs. However, the genome of the clonally propagating duckweed *Spirodela polyrhiza* (*Lemnaceae*) has low levels of DNA methylation, very low expression of RdDM components, and near absence of 24 nt siRNAs. Moreover, some genes encoding RdDM factors, DNA methylation maintenance, and RNA silencing mechanisms are missing from the genome. Here, we investigated the distribution of TEs and their epigenetic marks in the *Spirodela* genome. Although abundant degenerated TEs have largely lost DNA methylation and H3K9me2 is low, they remain marked by the heterochromatin-associated H3K9mel and H3K27mel modifications. In contrast, we find high levels of DNA methylation and H3K9me2 in the relatively few intact TEs, which are source of 24 nt siRNAs, like RdDM-controlled TEs in other angiosperms. The data suggest that, potentially as adaptation to vegetative propagation, RdDM extent, silencing components, and targets are different from other angiosperms, preferentially focused on potentially intact TEs. It also provides evidence for heterochromatin maintenance independently of DNA methylation in flowering plants. These discoveries highlight the diversity of silencing mechanisms that exist in plants and the importance of using disparate model species to discover these mechanisms.

[Supplemental material is available for this article.]

Transposable elements (TEs), or transposons, are mobile genetic elements that can change location and generate new copies in their host genomes. As a result, TEs populate eukaryotic genomes and can contribute to a significant fraction of their nuclear DNA (Wells and Feschotte 2020). Owing to their mobile nature, TEs have an important role in evolution and genetic innovation, but also they pose a threat to the genome integrity (Biémont and Vieira 2006; Feschotte 2008). To control TEs, various mechanisms have evolved to prevent or reduce their mobility.

In eukaryotes, transcriptional gene silencing (TGS) of TEs relies on the deposition of chromatin modifications leading to the formation of compact chromatin states, collectively known as heterochromatin, incompatible with canonical Pol II transcription (Allshire and Madhani 2018). Heterochromatin is generally characterized by repressive epigenetic marks, prominently DNA methylation (5′methylcytosine [5mC]), histone modifications such as histone H3 lysine-9 mono- and dimethylation (H3K9me1/H3K9me2, constitutive heterochromatin) or histone H3 lysine-27 triple methylation H3K27me3 (facultative or developmentally regulated heterochromatin), and the presence of specific histone variants (Henikoff and Smith 2015; Jamge et al. 2023). Upon silencing, TEs accumulate mutations and degenerate into nonautonomous TEs and fragmented remnants or relics (Blumenstiel 2019). Despite their inability to mobilize, degenerated TEs provide alternative DNA and RNA regulatory sequences (e.g., transcription factor binding sites, splicing information, transcriptional start or termination sites) or induce recombination owing to their repetitiveness (Ito et al. 2011; Kim and Zilberman 2014; Zervudacki et al. 2018; Sammarco et al. 2022; Ilık et al. 2024). Therefore, maintaining epigenetic control is important even for degenerated TEs, and in consequence, TE abundance and location largely shape the epigenetic landscape of genomes (Houben et al. 2003; Seymour et al. 2014; Sigman and Slotkin 2016; Wyler et al. 2020; Klein and Anderson 2022).

Another conserved mechanism to suppress TEs and maintain their epigenetic silencing depends on ~18–30 nucleotide (nt) long small RNAs (sRNAs) and members of the ARGONAUTE (AGO) protein family. Loaded into AGOs, TGS-associated sRNAs guide chromatin modifying complexes to TEs through sequence complementarity (Malone and Hannon 2009; Moazed 2009). In flowering plants (angiosperms), TE silencing is mostly associated with DNA methylation and H3K9me2, and the mechanism by which sRNAs guide chromatin modifications is known as RNA-directed DNA methylation (RdDM). Best studied in *Arabidopsis thaliana*,

[3]**These two authors contributed equally to this work.**
[4]**Present address: Biology School, Costa Rica University, San José 11501-2060, Costa Rica**
Corresponding author: arturo.mari-ordonez@gmi.oeaw.ac.at
Article published online before print. Article, supplemental material, and publication date are at https://www.genome.org/cgi/doi/10.1101/gr.279532.124. Freely available online through the *Genome Research* Open Access option.

during RdDM, H3K9me2 and DNA methylation recruit the plant-specific RNA polymerases (Pol) IV and V. Pol IV transcripts are processed into 24 nt siRNAs, which, loaded into members of the AGO4/6 clade, target Pol V transcripts to guide the sequence-specific deposition of DNA methylation in all cytosine contexts (CG, CHG, and CHH, where H is any nucleotide but G). Once established, DNA methylation can reinforce the deposition of H3K9me2 through the action of SUPRESSOR OF VARIEGATION 3–9 HOMOLOG (SUVH) family H3K9 methyltransferases, which can read DNA methylation. In turn, CHROMO-METHYL TRANSFERASE (CMT) 3 and 2 can bind to H3K9me2 to mediate CHG and CHH methylation, respectively. This results in a self-reinforcing loop between non-CG methylation and H3K9me2 independent of siRNAs. Symmetrical CG methylation is maintained across cell divisions through the action of METHYLTRANSFERASE 1 (MET1), recruited to hemi-methylated CG sites after DNA replication by VARIANT IN METHYLATION (VIM) proteins (for reviews, see Erdmann and Picard 2020; Tirot et al. 2021). Loss of RdDM, 5mC, or H3K9me2 results in the transcriptional reactivation of TEs (Mirouze et al. 2009; Tsukahara et al. 2010; Stroud et al. 2014; He et al. 2021; Osakabe et al. 2021). Therefore, DNA methylation, together with H3K9me2 and in cooperation with sRNAs, keeps TEs silenced.

Loss of TE control in somatic tissue is likely less deleterious as long as it does not affect the germline or, in plants, stem cells in the meristems or gamete precursor cells giving rise to the next generation, in which stability of the genome is highly relevant. In accordance, sRNA-guided TGS pathways are prominently active in reproductive tissues and silence active TEs encountered during fertilization (Bourc'his and Voinnet 2010; Marí-Ordóñez et al. 2013; Parhad and Theurkauf 2019). However, unlike in metazoans, in which such pathways are predominantly active in the gonads, in most flowering plants RdDM is not constrained to reproductive organs. The 24 nt siRNAs are also present in vegetative, somatic organs such as leaves or roots across all developmental stages (Havecker et al. 2010; Patel et al. 2021; Zhou et al. 2022), with interesting exceptions of the aquatic dicot carnivorous plant *Utricularia gibba* (L.) and the monocot *Spirodela polyrhiza* (L.) Schleid. Both contain much fewer 24 nt siRNAs and display reduced genome-wide levels of DNA methylation in vegetative tissues compared with other angiosperms (Michael et al. 2017; Fourounjian et al. 2019; Cervantes-Pérez et al. 2021). Although in the *U. gibba* such features can be a consequence of low TE content as repeats represent <3% of genome (Ibarra-Laclette et al. 2013), the TE content of the *Spirodela* genome is similar to that of *Arabidopsis* (~20%) (Wang et al. 2014). Therefore, reduced genomic TE load is unlikely to be the cause behind the low levels of DNA methylation and sRNAs in *Spirodela*. Furthermore, in *Spirodela*, several sRNA silencing components including some involved in RdDM have been shown to be missing, low, or not expressed. In addition, CMT2, which maintains CHH methylation, is lost in duckweeds (An et al. 2019; Ernst et al. 2023; Harkess et al. 2024).

The *Spirodela* genus is the most basal of the *Lemnaceae* family (order Alismatales), a monophyletic group of free-floating freshwater monocot plants, commonly known as duckweeds, composed of five genera (*Spirodela*, *Landoltia*, *Lemna*, *Wolfiella*, and *Wolffia*) (Bog et al. 2019; Tippery et al. 2021). Comprised of a leaf-like structure known as a frond, ranging from ~2 cm to 1 mm, duckweeds display an evolutionary reduction and simplification of their body plan compared with most angiosperms, including vestigiality and loss of organs such as roots and vasculature (Landolt 1986; Lemon and Posluszny 2000; Lam and Michael 2022; Ware et al. 2023). Although flowering and seed production has been reported, it is rare in most species (Landolt 1986; Pieterse 2013; Fourounjian et al. 2021). Duckweeds mostly propagate through rapid clonal reproduction (doubling of individuals ~1–5 days) known as vegetative budding: New fronds originate from budding pockets where meristems containing stem cells are located (Landolt 1986; Ziegler et al. 2015). Mother fronds (MFs) continuously give rise to daughter fronds (DF), which carry grand-daughter fronds (GDF) in their budding pockets even before detaching from the MF (Landolt 1986; Lemon and Posluszny 2000). This extremely efficient amplification of somatic tissue, omitting regular sexual propagation, and the free-floating way of living make *Spirodela* a unique model to explore if the differences in epigenetic parameters are connected with these differences in lifestyle compared with other angiosperms. Thus, the aim of this study is to investigate the TE silencing landscape in *S. polyrhiza* by profiling its genetic composition of silencing pathways, sRNAs, and epigenetic modifications commonly associated with TE control in angiosperms.

Results

Genome sequencing of *S. polyrhiza* 9509 from the Landolt collection

The genomes of several *S. polyrhiza* accessions (clones) have been sequenced (Wang et al. 2014; Michael et al. 2017; Xu et al. 2019), including a high-resolution reference genome assembly of its 20 chromosomes from the *S. polyrhiza* 9509 (Sp9509) and 7498 (Sp7498) clones (Michael et al. 2017; Hoang et al. 2018; Harkess et al. 2021). For our study, we retrieved Sp9509 from the Landolt duckweed collection, now managed at the Institute of Agriculture Biology and Biotechnology (IABB; CNR) (Morello et al. 2024). We performed 88× coverage short-read Illumina genome sequencing to account for potential genetic differences owing to independent clonal propagation over thousands of generations between this accession and that of the Rutgers Duckweed Stock Cooperative (RDSC) used to generate the reference genome (Hoang et al. 2018). The Landolt Sp9509 genome showed about 163,000 indels and about 512,000 SNPs (~0.4% of the *Spirodela* genome) compared with the Sp9509 reference (Supplemental Fig. S1). Given our special interest on TEs, we performed a de novo TE annotation using a combination of EDTA and RepeatModeler2 to identify repeats that were then further classified using DeepTE (Ou et al. 2019; Flynn et al. 2020; Yan et al. 2020).

To explore the TE silencing landscape during *Spirodela* asexual clonal reproduction, we used *Arabidopsis* as a comparative system to investigate *Spirodela* TE-derived sRNAs, TE epigenetic marks, and the genetic composition and expression of silencing pathways. Although TE regulatory mechanisms might differ between the two species given their evolutionary distance (Supplemental Fig. S2), we choose *Arabidopsis* as its silencing pathways and epigenetic mechanisms are well characterized by molecular and genetic means. Furthermore, the two species display similar genome size and TE content (Fig. 1A).

AGO-loaded sRNA and DNA methylation patterns imply low RdDM activity in *Spirodela*

Given that 24 nt sRNAs are considered one of the hallmarks of RdDM, we first compared the sRNA profiles of *Spirodela* confluent cultures (including fronds in all developmental stages) to those of

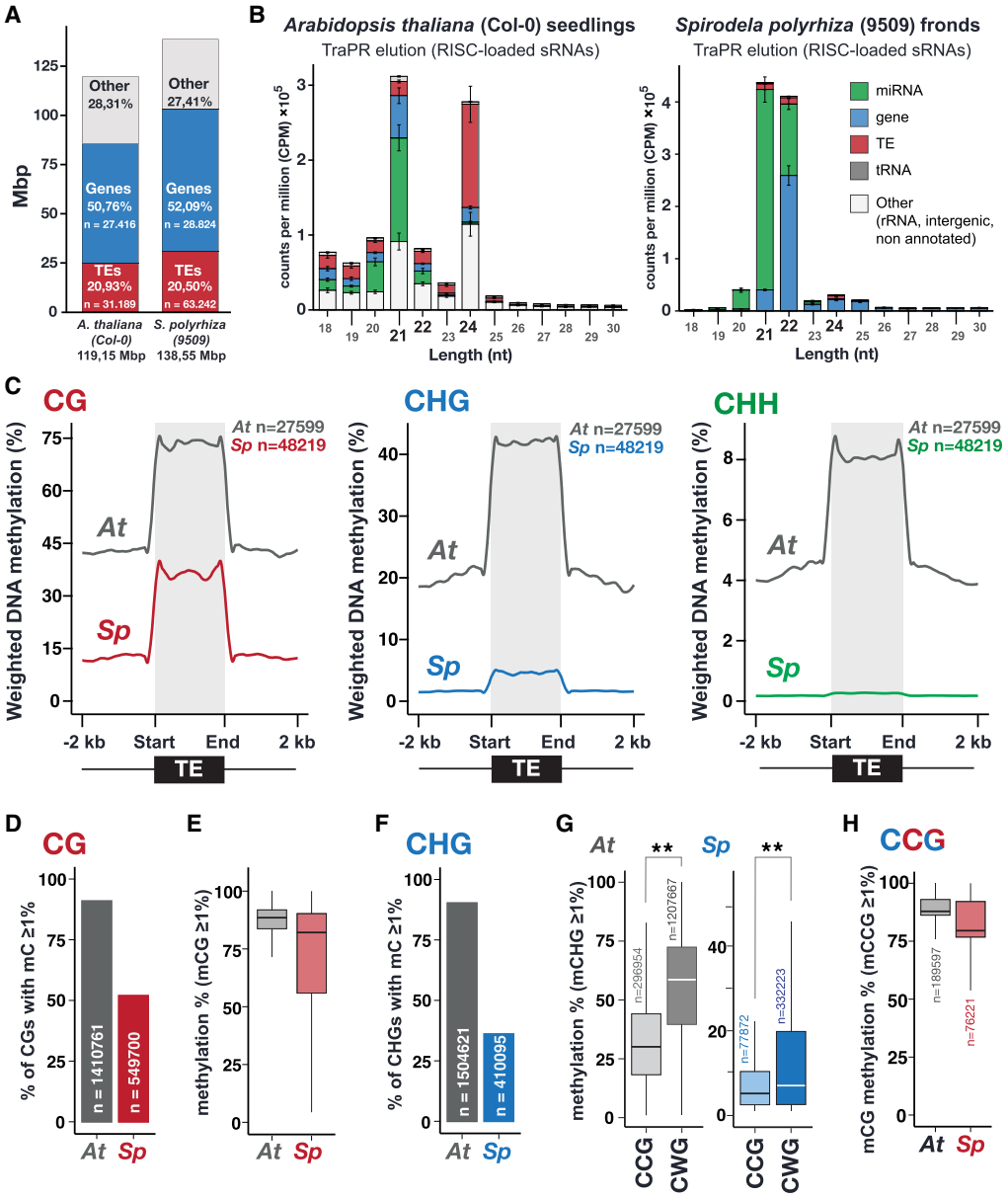

Figure 1. *Spirodela polyrhiza* sRNA and DNA methylation patterns. (*A*) Genome size, number, and genomic occupancy of genes and TEs in *Spirodela* and *Arabidopsis*. (*B*) Size distribution and genomic feature annotation of TraPR-purified sRNA from *Arabidopsis* and *Spirodela*. Error bars represent SD of the mean of three biological replicates. (*C*) Metaplots of averaged weighted DNA methylation in all three contexts (CG, CHG, and CHH, where H is any but G) over transposons (TEs; ≥100 bp) and 2 kb flanking regions in *Arabidopsis* and *Spirodela*. (*D*) Number and percentage of transposon CG sites displaying methylation levels ≥1% in *Arabidopsis* and *Spirodela*. (*E*) DNA methylation levels at CG sites from *D*. (*F*) Number and percentage of transposon CHG sites displaying methylation levels ≥1% in *Arabidopsis* and *Spirodela*. (*G*) DNA methylation levels at CCG and CWG in *Arabidopsis* and *Spirodela*. (*H*) Inner 5mC (CmCG) DNA methylation levels at CCG sites with outer 5mC (mCCG) ≥1% in *Arabidopsis* and *Spirodela*. (**) *P*-value < 2.22×10^{-16} (Wilcoxon rank-sum test). In all box plots, the median is indicated by a solid bar; the boxes extend from the first to the third quartile; and whiskers stretch to the furthest value within 1.5 times the interquartile range. (At) *Arabidopsis*, (Sp) *Spirodela*.

10-day-old *Arabidopsis* seedlings as the closest equivalent developmental stage. As sRNAs on the 21–24 nt range were very low in abundance in profiles generated from total RNA (Supplemental Fig. S3), we enriched our sRNA libraries by investigating AGO-loaded sRNAs using TraPR (Grentzinger et al. 2020). In contrast to *Arabidopsis*, in which AGO-loaded TE-derived 24 nt siRNAs are highly abundant, the *Spirodela* TraPR profile displays very low levels of 24 nt siRNAs, and it is dominated by 21–22 nt sRNAs (Fig. 1B; Supplemental Fig. S3), predominantly contributed by regulatory microRNAs (miRNAs). The lack of 24 nt siRNAs in the *Spirodela* TraPR profile is more pronounced than their loss in the *Arabidopsis* RdDM siRNA biogenesis-defective Pol IV mutant (*nrpd1*) (Supplemental Fig. S3; Teixeira et al. 2009; Nuthikattu et al. 2013; Creasey et al. 2014) Hence, low levels of AGO-loaded 24 nt siRNAs in *Spirodela* are compatible with the reduced or lack of RdDM activity at TEs during its asexual clonal growth.

Given the connection between sRNAs and DNA methylation, we next investigated *Spirodela* DNA methylation patterns. Methylome analysis by enzymatic methyl-seq (EM-seq) (Feng et al. 2020) showed similar results to those previously published using bisulfite sequencing (Michael et al. 2017). TE 5mC in all contexts is lower in *Spirodela* compared to *Arabidopsis*, with very low mCHG levels and hardly any mCHH (Fig. 1C). This is in agreement with the partial dependency of mCHH on 24 nt siRNAs. In addition, *Spirodela* lacks gene body CG methylation (gbM) (Supplemental Fig. S4A; Michael et al. 2017; Harkess et al. 2024). Although the role of gbM is unclear, it generally associates with highly expressed genes. In contrast, mCG near the transcription start site (TSS) is associated with gene silencing (Niederhuth et al. 2016; Bewick and Schmitz 2017). Although expressed genes do not display gbM, like in *Arabidopsis*, mCG around the TSS is higher in nonexpressed genes of *Spirodela* (Supplemental Fig. S4B,C), indicating that mCG in gene regulatory sequences influences transcription also in *Spirodela*.

CG and CHG methylation signatures are compatible with functional maintenance of DNA methylation independently of sRNAs

Once established, DNA methylation can be further maintained independently of sRNAs through several pathways depending on the sequence context (Mathieu et al. 2007; Cokus et al. 2008; Reinders et al. 2009) In *Spirodela*, the ratio of mCG sites at TEs (51.9%) is nearly half of that in *Arabidopsis* (90.9%) (Fig. 1D). However, at CG sites with 5mC levels ≥1%, mCG is similarly stable as in *Arabidopsis*, displaying median methylation levels >80% (Fig. 1E), although a higher variation was observed for *Spirodela* than *Arabidopsis*. Hence, the reduced global mCG level at TEs in *Spirodela* is the result of less individual CG sites being methylated.

As for mCG, the number of mCHG sites at TEs is much lower in *Spirodela* (36.1%) than in *Arabidopsis* (90.3%) (Fig. 1F). CHG sites can be further divided into CCG and CWG (CAG/CTG) subcontexts. In *Arabidopsis*, mCWG is higher than mCCG (Fig. 1G) owing to the combined differential affinities of SUVH4/5/6 and CMT3 to read and methylate individual cytosine sequence contexts (Cokus et al. 2008; Gouil and Baulcombe 2016; Li et al. 2018; Fang et al. 2022). This applies also to *Spirodela*, although methylation in both subcontexts is lower than in *Arabidopsis* (Fig. 1G). Furthermore, maintenance in the mCCG subcontext relies additionally on MET1. Being both CG and CHG contexts, methylated CCG sites are generally observed as mCmCG owing to the outer cytosine methylation (mCCG) being largely dependent on the internal CG methylation (CmCG) mediated by MET1 (Stroud et al. 2013; Yaari et al. 2015; Gouil and Baulcombe 2016; Li et al. 2018). Consequently, mCCG sites in *Arabidopsis* display a high internal CG methylation level, a pattern also observed in *Spirodela* (Fig. 1H). The similar mCHG patterns between the two species indicate that the responsible enzymes, SUVHs and ZMET, the CMT3 homolog in monocots (Bewick et al. 2017), probably share the same sequence preference, albeit their activity seems to be lower than in *Arabidopsis*. Nonetheless, given that CMT3/ZMET has been shown to be involved in gbM (Bewick et al. 2016; Niederhuth et al. 2016; Wendte et al. 2019), lower mCHG and lack of gbM in *Spirodela* might be related.

Altogether, our analysis indicates that mCG and mCHG maintenance mechanisms in *Spirodela* might operate in a similar fashion as in *Arabidopsis*. However, although low mCG is a consequence of reduced number of CG sites being methylated, low mCHG appears to be the combined result of lower number of targeted CHG sites and decreased maintenance activity.

Genetic composition and expression of silencing pathways partially account for sRNAs and DNA methylation features in *Spirodela*

In addition to low signatures of RdDM in *Spirodela*, coding potential for several of its components have been shown to be missing (An et al. 2019; Ernst et al. 2023; Harkess et al. 2024). To gain further insights on why levels of 24 nt siRNA and DNA methylation are reduced, we set to identify and examine the expression of known core components of angiosperm silencing pathways in *S. polyrhiza* (Fig. 2; Supplemental Fig. S5). The identification of orthologs and paralogs in the genome of Sp9509 was based on the presence of conserved functional domains. Annotations were further curated based on phylogeny trees built with proteins from several angiosperms and the prediction of known key domains and their organization (Supplemental Figs. S6–S18). For gene expression, we performed short-read transcriptome analysis in *Spirodela* and compared it to that of recently published *Arabidopsis* seedlings (Fig. 2; Li et al. 2023b). We further performed long-read cDNA-seq with Pacific Biosciences (PacBio) full-length transcript isoform-sequencing (Iso-Seq) technology in *Spirodela* to validate and eventually improve gene model annotations.

As expected from the prevalence of miRNAs in the *Spirodela* TraPR analysis, conserved plant miRNA biogenesis factors (Zhan and Meyers 2023) are expressed at similar levels as those in *Arabidopsis* (Fig. 2A). Likewise, genes required for the production of regulatory 21 nt siRNA *trans*-acting (ta)siRNA (Yoshikawa et al. 2005; Liu et al. 2020)—SUPRESSOR OF GENE SILENCING 3 (SGS3), RNA-DEPENDENT RNA POLYMERASE 6 (RDR6), and DICER-LIKE 4 (DCL4)—are present and expressed (Fig. 2B). *Spirodela* lacks many components, effectors, and regulators of 21–22 nt siRNA pathways, such as RNASE THREE-LIKE 1 (RTL1), DOUBLE-STRANDED RNA BINDING PROTEIN 7 (DRB7) (Shamandi et al. 2015; Montavon et al. 2017; Tschopp et al. 2017), and orthologs of the RDRγ clade highly conserved in plants and fungi (Fig. 2B; Supplemental Figs. S6, S7; Zong et al. 2009; Willmann et al. 2011). Gene absences also include the antiviral factors DICER-LIKE 2 (DCL2) and ARGONAUTE 2 (AGO2) (Fig. 2B,C; Supplemental Figs. S8, S9; Deleris et al. 2006; Garcia-Ruiz et al. 2010; Harvey et al. 2011; Carbonell et al. 2012). In contrast, two RDR1 and eight tandemly repeated copies of AGO5 are present (Fig. 2B,C; Supplemental Figs. S7, S9, S10). Both have been implicated in virus exclusion and TE silencing in meristems in *Arabidopsis* (Yu et al. 2003; Brosseau and Moffett 2015; Bradamante et al. 2023; Incarbone et al. 2023), and in monocots, AGO5 participates in anther development and TE silencing during male gametogenesis (Zhai et al. 2015; Fei et al. 2016; Lee et al. 2021).

Regarding the RdDM pathway, *Spirodela* contains the minimal set of its components, either with no or with a reduced number of paralogs compared with *Arabidopsis* (Fig. 2C,D). In *Spirodela*, SAWADEE HOMEODOMAIN HOMOLGUE 1 (SHH1), a dual reader for repressive H3K9me2 and unmethylated H3K4(me0), and the chromatin remodeler CLASSY 1/2 (CLSY1/2) are absent (Fig. 2D; Supplemental Figs. S11, S12). However, a single ortholog of CLSY3 was found in *Spirodela* (Fig. 2D; Supplemental Fig. S12). In *Arabidopsis*, the SHH1-CLSY1/2 module mainly recruits Pol IV to short TEs within gene-rich regions, whereas CLSY3 and its paralog CLSY4 recruit Pol IV to TE-rich pericentromeric regions in a SHH1-idependent but DNA methylation–dependent manner

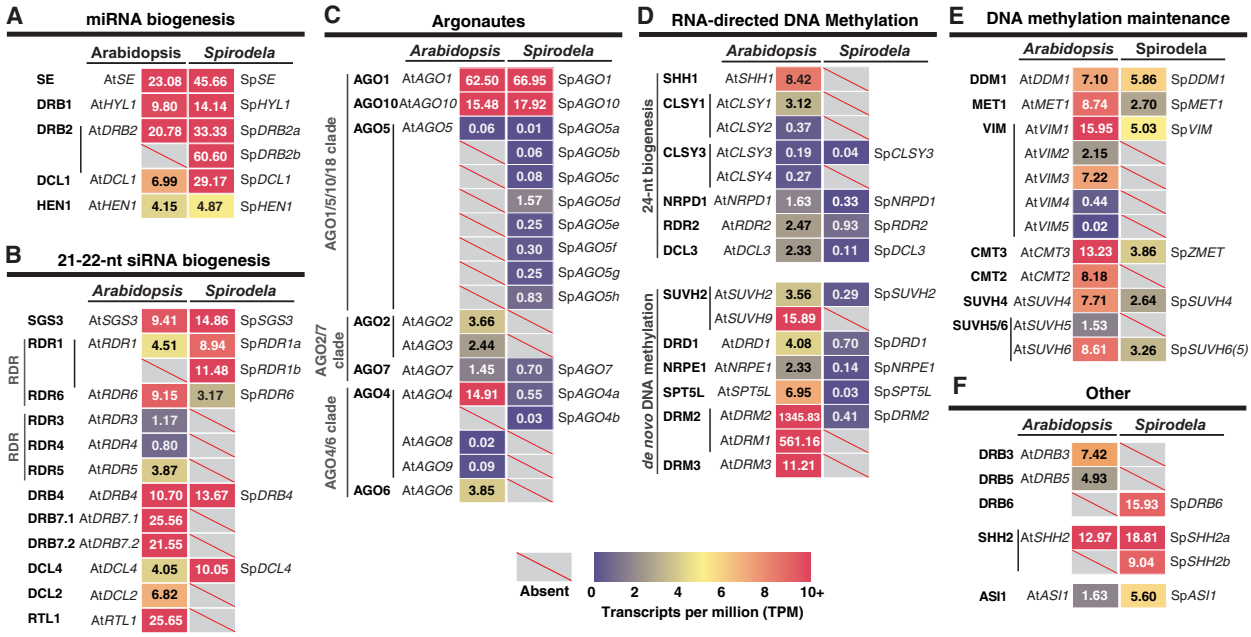

Figure 2. Genetic composition and expression of silencing pathways in *Spirodela*. (*A–F*) Expression in transcripts per million (TPM) of silencing components in *Arabidopsis* and their identified orthologs and paralogs in the *S. polyrhiza* 9509 (Sp9509) genome. Gene IDs for both *Arabidopsis* and *Spirodela* can be found in Supplemental Figure S5.

(Law et al. 2011, 2013; Zhou et al. 2018, 2022). However, *Spirodela* has two SHH2 orthologs (Fig. 2; Supplemental Fig. S11). Part of a nucleosome positioning complex during transcription initiation in *Arabidopsis* (Diego-Martin et al. 2022), in maize, SHH2 binds preferentially to H3K9me1 in vitro and interacts in vivo with both Pol IV and V in maize, possibly connecting RdDM to H3K9me1 installation (Haag et al. 2014; Wang et al. 2021).

Similarly, no AGO6 ortholog was found, yet two AGO4 are both required nonredundantly to maintain DNA methylation at most RdDM target loci in *Arabidopsis* (Fig. 2D; Supplemental Fig. S9; Duan et al. 2015). A single SUVH2 ortholog is present in *Spirodela* (Fig. 2D; Supplemental Fig. S13), which together with its paralog SUVH9 redundantly recruit Pol V to RdDM targets by binding to methylated DNA in *Arabidopsis* (Johnson et al. 2008, 2014; Liu et al. 2014). Regarding the RdDM-associated DNA methyltransferases, DOMAIN REARRANGED METHYLTRASFERASE (DRM) 2 but not DRM3 (a conserved catalytically inactive paralog that contributes to DRM2 activity) (Chan et al. 2004; Wierzbicki et al. 2009; Zhong et al. 2015; Liu et al. 2018; Fang et al. 2021) orthologs were found (Fig. 2D; Supplemental Fig. S14). Additionally, although NRPE1 (Pol V) and its partner SUPPRESSOR OF TY INSERTION-LIKE (SPT5L; a paralog of the general transcription elongation factor SPT5) are conserved in *Spirodela*, we noticed that both contain fewer tryptophan/glycine (GW/WG) repeats than those of other angiosperms (Fig. 2D; Supplemental Figs. S15, S16; El-Shami et al. 2007; Bies-Etheve et al. 2009; Rowley et al. 2011; Huang et al. 2015; Trujillo et al. 2016). GW/WG repeats, or AGO-hooks, allow AGO4/6 binding to Pol V to scan its nascent transcripts for positive siRNA matches to recruit DRM2. These, together with NRPD1, RDR2, DCL3, and the rest of conserved RdDM components, might suffice for a functional pathway in *Spirodela* (Fig. 2; Supplemental Figs. S7, S8, S12, S15). Nonetheless, their low expression levels (Fig. 2C,D) rationalize the low abundance of AGO-bound 24 nt siRNAs and associated CHH methylation during clonal propagation in *Spirodela* (Fig. 1B,C).

Lastly, we inspected DNA methylation maintenance pathways. As predicted from the patterns of mCG and mCHG (Fig. 1D–H), MET1, VIM (ORTH), CMT3/ZMET, SUVH4, SUVH5/6, and DECREASE IN DNA METHYLATION 1 (DDM1) orthologs were found present and expressed in *Spirodela*, albeit at a lower degree than in *Arabidopsis* (Fig. 2E; Supplemental Figs. S12–S14, S17). A single ortholog of the SUVH5/6 orthogroup was found in *Spirodela* (Fig. 2E; Supplemental Fig. S13). In *Arabidopsis*, SUVH5 and SUVH6 display different 5mC subcontext binding affinities as well as genomic targets (Johnson et al. 2007; Rajakumara et al. 2011; Li et al. 2018; Zhang et al. 2023). Absence of either could have implications for the DNA methylation landscape if their functions are conserved outside of *Arabidopsis*. The *Spirodela* SUVH5/6 otholog contains a conserved motif present in *Arabidopsis* SUVH6 but absent in SUVH5, required for interaction with ANTI-SILENCING 1 (ASI1) to regulate silencing at intronic TEs and expression of their host genes (Saze et al. 2013; Wang et al. 2013; Duan et al. 2017; Zhang et al. 2023). As an ASI1 ortholog was also found in *Spirodela* (Fig. 2F; Supplemental Fig. S18), we named the *Spirodela* SUVH5/6 ortholog as spSUVH6(5) until its sequence binding preference is determined. In addition, with regards to mCHH maintenance, CMT2, required to maintain mCHH together with SUVH4 (Stroud et al. 2014), is missing like in maize (Bewick et al. 2017), as previously reported (Fig. 2E; Supplemental Figs. S13, S14; Harkess et al. 2024).

Thus, reduced 24 nt siRNA and mCHH levels in *Spirodela* can be explained by the combined reduction in RdDM composition and expression in addition to the absence of CMT2. However, it does not account for the global decrease in mCG and mCHG as their maintenance pathways seem intact and expressed in *Spirodela*.

Few TEs from different superfamilies display high levels of DNA methylation in *Spirodela*

To further gain insight into the patterns of TE DNA methylation, we examined its distribution along the *Spirodela* genome. To exclude any confounding effects of gbM, we calculated mean DNA methylation levels exclusively on TEs and their density in 100 kb windows. At gene-rich regions, DNA methylation is very scarce (Fig. 3A; Supplemental Fig. S19A). As in *Arabidopsis*, *Spirodela* DNA methylation is concentrated at TE-dense regions (presumably centromeric and pericentromeric domains). However, not all TE-dense regions are highly methylated (Supplemental Fig. S19B). Hence, we investigated if local DNA methylation levels correlate with TE density as in other angiosperms (Zhang et al. 2006; Regulski et al. 2013; Seymour et al. 2014; Wyler et al. 2020). At equal TE-content, DNA methylation is lower in all contexts in *Spirodela* compared with *Arabidopsis*, especially at CHG and CHH (Fig. 3B; Supplemental Fig. S20A). Moreover, at the CG context, *Spirodela* displays a broad variation range for a given TE content: Even at TE densities >50%, average mCG still spans between 0% and 75% (Fig. 3B).

To address the origin of such variation, we investigated the DNA methylation levels of individual TEs. This revealed that the majority of TEs in *Spirodela* display low or very low levels of DNA methylation in all contexts, especially CHG and CHH (Fig. 3C; Supplemental Fig. S20B,C). Nonetheless, despite this substantially reduced DNA methylation, increased expression at TEs was not observed (Fig. 3D; Supplemental Fig. S20D). TEs with high or low DNA methylation levels did not belong to any specific TE class or superfamily. For all the main plant TE superfamilies (for summary of TE classification and codes used here, see Supplemental Fig. S21; Wicker et al. 2007), DNA methylation was nearly absent except for a few elements (Fig. 3E). Thus, low genome-wide methylation levels in *Spirodela* result from only a few methylated TEs, although these can display high mCG levels similar to those found in *Arabidopsis* (Fig. 3C,E).

Potentially intact transposons are the conspicuous targets of DNA methylation in *Spirodela*

Although TE location and density influences their epigenetic regulation (Sigman and Slotkin 2016), in *Arabidopsis* and the tomato, DNA methylation of longer, evolutionary younger, and therefore potentially autonomous TE insertions are differentially regulated than often fragmented TE relics resulting from the accumulation of mutations and truncations over evolutionary times following their silencing (Sigman and Slotkin 2016; Blumenstiel 2019; Zattera and Bruschi 2022). On one hand, DNA methylation in long TEs is maintained by a combination of RdDM acting on their boundaries (mainly in young active TEs) and CMT activity along their body. On the other hand, short, degenerated TE remnants do not need CMT to maintain their methylation (Zhong et al. 2012; Zemach et al. 2013; Wang and Baulcombe 2020). To explore if TE length influences DNA methylation in *Spirodela*, we sorted TEs into short TE fragments (100 to 500 bp), intermediate TEs (0.5 to 4 kb), and long TEs (>4 kb). This revealed that only long TEs are heavily methylated at CG and, to a lesser extent, in CHG. Intermediate TEs display a wide range of mCG levels, whereas TE fragments are minimally or not methylated (Fig. 4A).

To further explore the connection between TE length and DNA methylation, we focused on the two superfamilies of long terminal repeat (LTR) retroelements (RTEs): *Ty1/Copia* (RLC) and *Ty3/Gypsy* (RLG). LTR-RTEs are the most abundant class of TEs in the *Spirodela* genome, collectively representing >50% of the TE fraction of the genome and largely contributing as well to that of *Arabidopsis* (Fig. 4B; Supplemental Fig. S22). In addition, the genetic structure and domain organization of complete functional elements are well known (Kumar and Bennetzen 1999; Gorinšek et al. 2004; Neumann et al. 2019). Thus, LTR-RTEs offer a good case study to investigate any link between DNA methylation and TE length, using the latter as a proxy for their completeness and potential autonomy for transposition under the assumption that degenerated and fragmented shorter TEs have lost some or all the required domains to mobilize autonomously (nonautonomous elements) (Blumenstiel 2019). For better resolution, we split TE sizes into further size categories in the intermediary range between 0.5 and 4 kb. Within each size bin, *Spirodela* DNA methylation is lower than in *Arabidopsis*. However, in *Spirodela*, the average mCG and mCHG gradually increase with TE size, although mCHG does not achieve levels comparable to those of *Arabidopsis* (Fig. 4C, D; Supplemental Fig. S23A,B). The proportion of TEs displaying high CG methylation rises across TE-size groups. Although very few TE-fragments <500 bp are highly methylated, the majority of long TEs (>4 kb) have mCG >60% (Fig. 4C,D). At the same time, the fraction of TEs with at least one intact cognate protein domain and the number of domains identified per TE annotation increases with each size category, with the majority of long LTR-RTEs containing all domains associated with each superfamily (Fig. 4E,F).

Therefore, in *Spirodela*, most potentially intact TEs display high levels of DNA methylation, which decreased as they degenerated and decayed. Given that long intact LTR-RTEs represent a minority of *Spirodela* TEs (Supplemental Fig. S23C,D), their low abundance helps explain the few TE numbers with high DNA methylation (Fig. 3C,E). In addition, the proportion of hypomethylated shorter LTR-RTE fragments relative to methylated intact TEs is higher in *Spirodela* than in *Arabidopsis* (Fig. 4G,H; Supplemental Fig. S23E,F), resulting in the global reduction of TE methylation (Figs. 1E, 3A,B).

Levels of H3K9me2, but not H3K9me1, are reduced in *Spirodela*

Considering the association between DNA and H3K9 methylation in plants, we explored how far DNA methylation in *Spirodela* would impact the histone methylation landscape. H3K9me2 and H3K9me1 are commonly linked with heterochromatin formation at silenced TEs (Jackson et al. 2004; Fuchs et al. 2006; Stroud et al. 2014; Jamge et al. 2023). Western blot analysis revealed that the H3K9me2 level in *Spirodela* is lower than in *Arabidopsis*, whereas H3K9me1 displayed similar levels (Fig. 5A). This was unexpected as we anticipated in *Spirodela* a decrease of both marks, given their connection with DNA methylation and reduction upon loss of non-CG methylation in *Arabidopsis* (Stroud et al. 2014; Choi et al. 2021). To corroborate the observation, we investigated histone post-translational modifications (PTMs) by mass spectrometry (Johnson et al. 2004; Scheid et al. 2022), which confirmed an approximately eight- to 10-times-lower level of H3K9me2 but similar H3K9me1 levels in *Spirodela* relative to *Arabidopsis* (Supplemental Fig. S24).

A low proportion of TEs show high H3K9me2 enrichment in *Spirodela*

To further delve into the distribution of H3K9me1/2 in *Spirodela* and how the general organization of heterochromatic marks is affected by its reduced DNA methylation levels, we performed chromatin immunoprecipitation (ChIP) in *Spirodela* fronds and

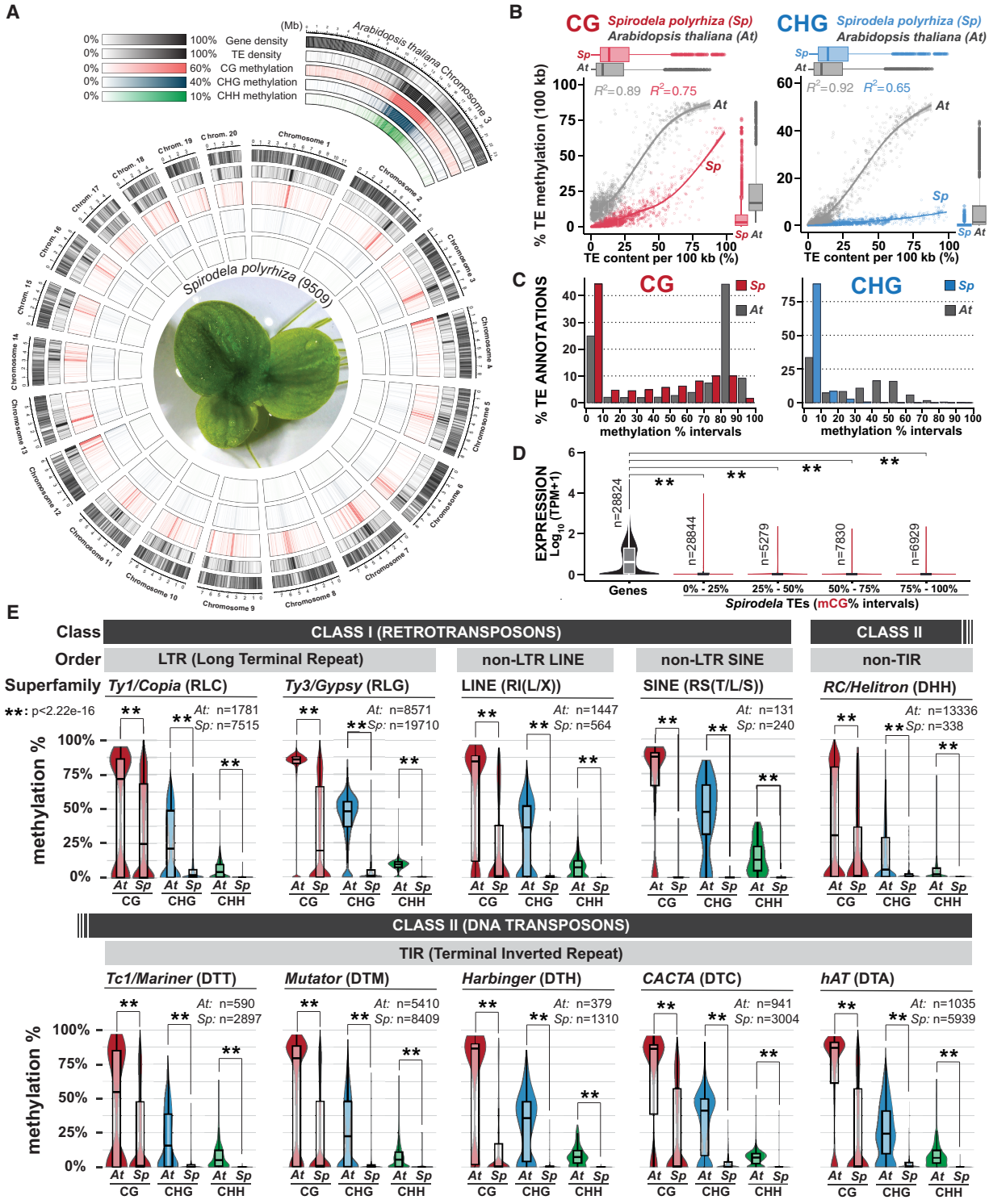

Figure 3. Distribution of DNA methylation in *Spirodela* chromosomes and TEs. (*A*) Circos plot (Krzywinski et al. 2009) of genome-wide distribution of DNA methylation densities by chromosome in *Spirodela*. From outside to inside: gene density; TE density; and CG, CHG, and CHH methylation. Mean DNA methylation, gene, and TE density values within the indicated ranges are displayed for 100 kbp intervals in 50 kbp sliding windows. *Arabidopsis* Chromosome 3 is shown for comparison. (*B*) Scatter plot and best fit line of average TE CG and CHG DNA methylation against TE content per 100 kb genomic bins in *Arabidopsis* and *Spirodela*. Colored shadows indicate the SEM. (*C*) Bar plot of the distribution (%) of TE annotations (≥100 bp) within 10% incremental intervals of CG and CHG methylation in *Arabidopsis* and *Spirodela*. (*D*) Analysis of *Spirodela* TE expression within 25% incremental intervals of CG methylation. Global gene expression values are shown for comparison. (*E*) Distribution of CG, CHG, and CHH methylation across the main TE superfamilies in *Arabidopsis* and *Spirodela*. The number of TE annotations belonging to each superfamily by species is indicated (n). (**) *P*-value < 2.22×10^{-16} (Wilcoxon rank-sum test). In box plots, median is indicated by solid bar; the boxes extend from the first to the third quartile, and whiskers stretch to the furthest value within 1.5 times the interquartile range. (At) *Arabidopsis*, (Sp) *Spirodela*.

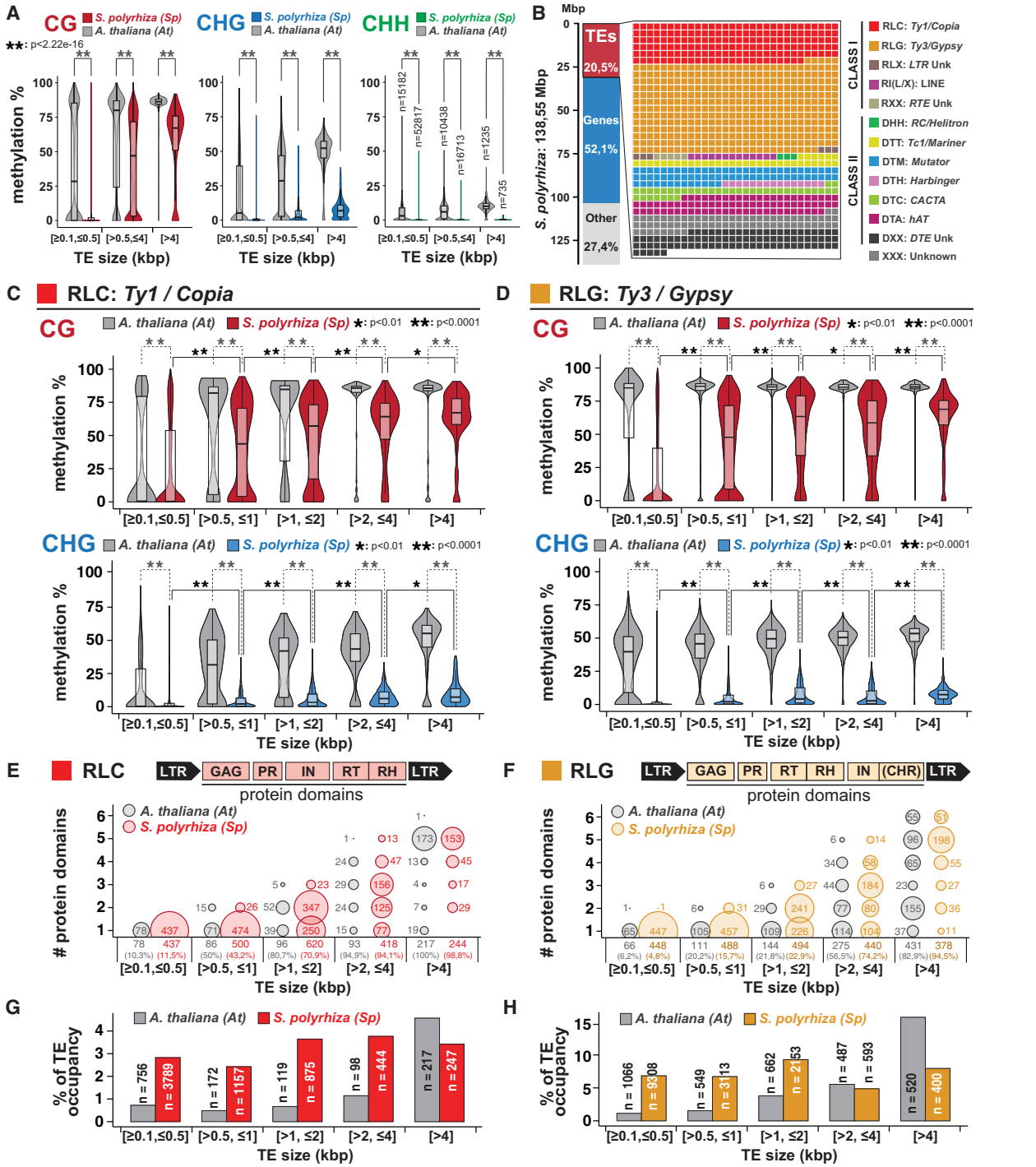

Figure 4. Length-dependent TE DNA methylation in *Spirodela polyrhiza*. (*A*) CHG and CHH methylation levels (%) across all TEs (≥100 bp) in *Arabidopsis* and *Spirodela* split by size into short (≥100 bp, <500 bp), intermediate (>500 bp, ≤4 kbp), and long (>4 kbp). Number values for each size category in each genome is indicated within the plot for mCHH. (*B*) Waffle chart of the relative contribution of different TE superfamilies over the total genomic space occupied by TEs in *Spirodela*. (*C*,*D*) CG and CHG methylation levels (%) between different length range groups for RLC: *Ty1/Copia* (*C*) and RLG: *Ty3/Gypsy* (*D*) in *Arabidopsis* and *Spirodela*. Number values are indicated in panels *G* and *H*. (*E*,*F*) Presence and number of RCL (*E*) and RLG (*F*) TE protein domains, determined by TEsorter, across TE annotations of varying sizes in *Arabidopsis* and *Spirodela*. Bubble plots depict domain count distributions for TEs with at least one domain. Numbers *above* the TE size category denotes TE annotations with at least one domain, with percentages shown in brackets relative to total TE annotations per size category. (*G*,*H*). Bubble size is relative to the number of TEs (indicated within or next to the bubble). Schematic representation of RLC and RLG protein and domain structure is included on *top* of each plot. (GAG) Nucleocapsid, (PR) protease, (IN) integrase, (RT) reverse transcriptase, (RH) RNase H, and (CHR) chromodomain, present only in the *Chromoviridae* genus of RLG. (*G*,*H*) Number of TE annotations and relative contribution to total genomic TE load (TE occupancy %) at each size category for RLC (*G*) and RLG (*H*). (*) *P*-value < 0.01, (**) *P*-value < 0.0001 (Wilcoxon rank-sum test). In all box plots, the median is indicated by solid bar; the boxes extend from the first to the third quartile; and whiskers stretch to the furthest value within 1.5 times the interquartile range. (At) *Arabidopsis*, (Sp) *Spirodela*.

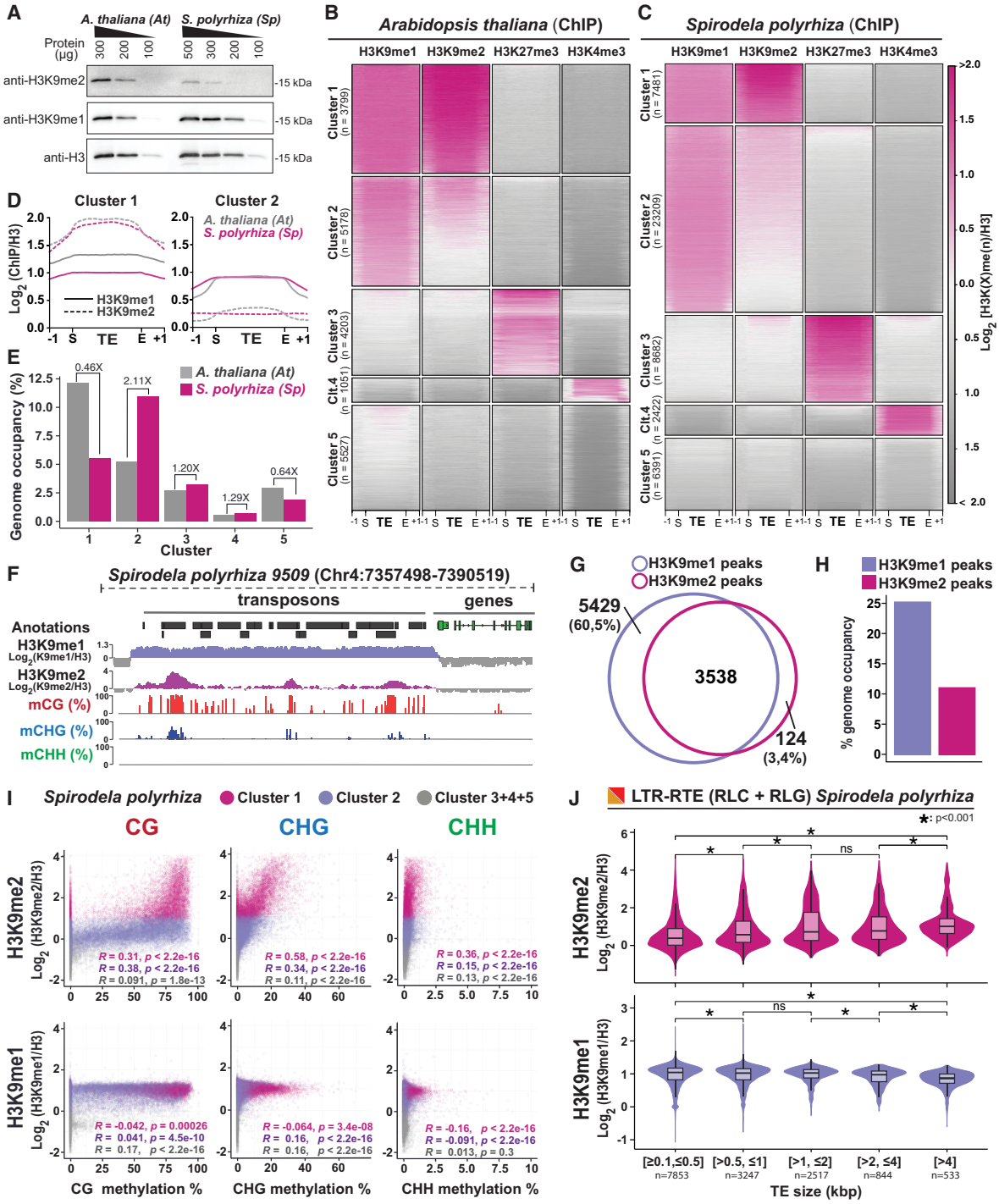

Figure 5. Patterns of H3K9me1/2 distribution in *S. polyrhiza* transposons. (*A*) Protein blot analysis of H3K9me1 and H3K9me2 abundance in *Spirodela* compared with *Arabidopsis* at different protein amounts (micrograms). Total H3 protein levels are shown as loading control. (*B*,*C*) Heatmap of *k*-means clustering of transposons in *Arabidopsis* (*B*) and *Spirodela* (*C*) using H3K9me1, H3K9me2, H3K27me3, and H3K4me3 enrichment over H3, presented as $\log_2$[ChIP(X)/ChIP(H3)]. Enrichment is represented by color, and depletion is shown in gray. Each row corresponds to a length-normalized TE annotation ± 1 kb. Transposons are grouped into clusters 1 to 5 based on the abundance of examined marks. (*D*) Metaplots of average weighted H3K9me1 (solid line) and H3K9me2 (dashed line) enrichments over H3 at cluster 1 and 2 transposons ± 1 kb in *Arabidopsis* (colored) and *Spirodela* (gray). (*E*) Relative genome (%) occupancy of each of the TE clusters defined in *B* and *C* in *Arabidopsis* (gray) and *Spirodela* (colored). (*F*) Genome browser capture of the distribution of H3K9me1 and H3K9me2 enrichments, together with DNA methylation, along genes and transposons in *Spirodela*. (*G*) Venn diagram of the overlap between H3K9me1 and H3K9me2 peaks along *Spirodela* genome. (*H*) Genome occupancy (%) of H3K9me1 and H3K9me2 in *Spirodela* genome. (*I*) Scatter plots of DNA methylation in all three contexts against H3K9me1 and H3K9me2 enrichments of TEs in cluster 1, 2, and 3+4+5 combined in *Spirodela*. *R* and *P* indicate Pearson correlation coefficients and *P*-values. (*J*) Analysis (violin and box plots) of H3K9me1 and H3K9me2 enrichments in different TE length groups for RLC and RLG combined in *Spirodela*. In all box plots, the mean is indicated by solid bar; the boxes extend from the first to the third quartile; and whiskers stretch to the furthest value within 1.5 times the interquartile range. (*) *P*-value < 0.001, (ns) not significant.

Arabidopsis 10-day-old seedlings (Supplemental Fig. S25) and focused on the association of these modifications with the TEs. In addition to H3, H3K9me1, and H3K9me2, we generated genomic profiles through ChIP-seq for H3K27me3 and H3K4me3. Although Polycomb-mediated H3K27me3 generally mediates developmentally regulated gene silencing, its association with TEs was investigated given that it also regulates TEs in the absence or loss of DNA methylation (Mathieu et al. 2005; Walter et al. 2016; Montgomery et al. 2020; Rougée et al. 2021) and may contribute directly to TE silencing (Hisanaga et al. 2023). H3K4me3, was taken as an euchromatic mark control (Houben et al. 2003; Zhang et al. 2009; Roudier et al. 2011; Ding et al. 2012; Pratx et al. 2023).

As observed for DNA methylation (Fig. 3A), H3K9me1/2 is concentrated at TE-dense regions in *Spirodela* (Supplemental Fig. S26), at likely centromeric and pericentromeric heterochromatic regions (Houben et al. 2003; Jackson et al. 2004; Harkess et al. 2024). The reduced size of such regions (spanning a few kilobase pairs per chromosome) (Supplemental Fig. S26) in *Spirodela*, compared with *Arabidopsis*, and larger pericentromeric regions (megabase pairs long) and their increased number (20 chromosomes in *Spirodela* in contrast to five in *Arabidopsis*) fit the speckled pattern of small dense DNA foci in DAPI staining of interphase nuclei of *Spirodela* (Supplemental Fig. S27). This is also compatible with previous observations of dispersed H3K9me2 foci in *Spirodela* nuclei immunostainings (Cao et al. 2015).

A more detailed *k*-means clustering analysis of histone mark profiles relative to H3 over TEs identified five clusters with similar features in both *Arabidopsis* and *Spirodela* (Fig. 5B,C). Clusters 1 and 2 contain TEs enriched for H3K9me1/2, whereas clusters 3 and 4 consist of those marked by H3K27me3 and H3K4me3 respectively. Lastly, cluster 5 encompasses TEs depleted of any of the profiled marks (Fig. 5B,C).

Although cluster 1 and 2 TEs are marked by H3K9me1/2, they display homogeneous H3K9me1 but contrasting H3K9me2 levels (Fig. 5D; Supplemental Fig. S28). TEs in cluster 1 are more enriched in H3K9me2 than in H3K9me1, whereas in cluster 2 TEs H3K9me2 is below H3K9me1 (Fig. 5D). The two clusters comprise very different fractions of the two genomes and TE space. In *Spirodela*, cluster 1 only comprises ~20% of the TE space, representing <6% of the genome, whereas in *Arabidopsis* is the most abundant one, encompassing ~35% of the TE space and ~12% of the genome. Cluster 2, on the contrary, occupies 45% of the *Spirodela* TE space (>10% of its genome) but only ~20% in *Arabidopsis* (5% of the genome) (Fig. 5E; Supplemental Fig. S29A).

Given the similar genome size and TE content in both species, the opposed contribution of cluster 1 and cluster 2 to their genomes is in line with the levels of H3K9me2 observed by western blot and mass spectrometry. Furthermore, similar H3K9me1 levels in both clusters concur with its even abundance in *Spirodela* and *Arabidopsis*. Hence, reduced DNA methylation levels in *Spirodela* correlate with a smaller fraction of the genome displaying a high H3K9me2 enrichment over TEs, but it does not impact H3K9me1 distribution, nor does it lead to a widespread compensatory regulation of TEs by H3K27me3. We noticed that despite cluster 3 occupying a comparable fraction of TE sequences in both species (Fig. 5E), *Spirodela*, in contrast to *Arabidopsis*, displays TE-rich regions devoid of DNA methylation and H3K9me1/2 but rich in H3K27me3 (e.g., Chromosomes 1, 6, 10, 14, 20) (Supplemental Fig. S26). No obvious differences in TE-superfamily composition were observed between cluster 3 and clusters 1 and 2 (Supplemental Fig. S29B), suggesting no particular TE superfamily is preferentially regulated by Polycomb.

H3K9me1 and H3K27me1 mark TEs independently of their length and methylation status in *Spirodela*

A closer inspection of the distribution of H3K9me1/2 along *Spirodela* TEs revealed that H3K9me1 uniformly covers TEs, whereas H3K9me2 peaks are found only at individual TEs (Fig. 5F). Furthermore, although >95% of H3K9me2 peaks overlapped with H3K9me1 domains, a significant fraction of H3K9me1 peaks (60,5%) did not with H3K9me2-associated regions (Fig. 5G). Moreover, most H3K9me2 peaks were embedded within H3K9me1 (Supplemental Fig. S29C). Adding to that, H3K9me1-enriched regions occupy 25% of the *Spirodela* genome, whereas H3K9me2 peaks represent <12% (Fig. 5H). This indicates that, similar to DNA methylation, high levels of H3K9me2 are only found within few TEs. Such observations prompted us to investigate the association between H3K9me1/2 and DNA methylation in *Spirodela*, and indeed, H3K9me2 levels in *Spirodela* positively correlate with DNA methylation, including mCHG, like in *Arabidopsis* (Fig. 5I; Supplemental Fig. S30). Parallel to DNA methylation (Fig. 3), H3K9me2 increased with TE size (Fig. 5J). This further supports that, as previously inferred, the positive feedback loop between mCHG and H3K9me2 operates in *Spirodela*. However, this did not apply to H3K9me1. Although in *Arabidopsis* TEs enriched in H3K9me1 invariably displayed high levels of DNA methylation (Supplemental Fig. S30), they did not so in *Spirodela* with its broad range of DNA methylation levels at TEs (Fig. 5I). Accordingly, H3K9me1 levels vary little across TE sizes (Fig. 5J).

These results indicate that, in *Spirodela*, H3K9me1 serves as broad TE mark but does not rely on DNA methylation as H3K9me2, suggesting that they might be differentially regulated. Although *Arabidopsis* H3K9 histone methyl-transferases (HMTs) can catalyze both H3K9me1 and me2 in vitro (Jackson et al. 2004; Ebbs and Bender 2006), it is unclear how their mono- and di-methyl-transferase activity is regulated in vivo or if both marks are deposited by the same HMTs. Loss of SUVH4, the main HMT in *Arabidopsis*, results in a strong reduction of H3K9me2 and loss of epigenetic silencing, only marginally affecting H3K9me1 and global heterochromatin organization (Jackson et al. 2002, 2004; Jasencakova et al. 2003). This originally led to the proposition that H3K9me2 and H3K9me1 play different roles in silencing and heterochromatin maintenance respectively (Jackson et al. 2004).

Given that heterochromatin maintenance is not only relevant for TE silencing by as well for genome stability, we sought to investigate the distribution of other epigenetic marks associated with heterochromatin and genome stability. Specifically, H3K27me1, which in plants is largely associated with maintenance of constitutive heterochromatin, especially during DNA replication, and its distribution are not affected by loss of mCG (Mathieu et al. 2005; Shi and Dawe 2006; Jacob et al. 2009; Sequeira-Mendes et al. 2014; Montgomery et al. 2020; Jamge et al. 2023). *Arabidopsis* mutants lacking H3K27me1 show not only loss of TE silencing but also defects in chromatin organization and excess of repetitive DNA owing to heterochromatin amplification during DNA replication (Jacob et al. 2009; Stroud et al. 2012; Dong et al. 2021). To study its distribution in *Spirodela*, we performed H3K27me1, along with H3K9me1/2, ChIP. The resulting profiles and *k*-means clustering analysis showed that H3K27me1 displays an overlapping pattern with H3K9me1, present at TEs independently of DNA methylation and occupying as well a large fraction of the genome (Supplemental Fig. S31). Hence, in *Spirodela*, despite the reduced levels of DNA methylation,

H3K9me2, H3K9me1, and H3K27me1 remain associated with TEs, likely to maintain heterochromatin and genome integrity.

5S rDNA also display low levels of DNA methylation and H3K9me1/2 in *Spirodela*

Besides TE silencing, DNA methylation, H3K9me2, and RdDM are also involved in the epigenetic regulation of other repeats in plants. To investigate if the unique patterns seen on TEs also affect other repeats in *Spirodela*, we looked into the epigenetic landscape of the *5S rDNA* repeats. Present in hundreds or thousands of copies clustered in several large tandem arrays, most *5S rDNA* repeats are generally silenced in *Arabidopsis* and are well-known targets of RdDM (Llave et al. 2002; Xie et al. 2004; Blevins et al. 2009; Simon et al. 2018). Although *Spirodela* and other duckweeds have been shown to have abnormally low numbers of *5s rDNA* repeats (fewer than 80–100 copies), two *5S rDNA* clusters in *S. polyrhiza* have been located on Chromosomes 6 and 13 (Hoang et al. 2018, 2020; Chen et al. 2021, 2024). A close inspection to the two *5S rDNA* clusters in *Spirodela* revealed clear differences with the epigenetic patterns found in *Arabidopsis* (Supplemental Fig. S32A). In *Spirodela*, *5S rRNA* repeats did not display DNA methylation in any context nor H3K9me1/2 and H3K27me1/3 enrichments (Supplemental Fig. S32B,C). Nonetheless, in *Spirodela*, 24 nt siRNAs also mapped to *5S rDNA* repeats (Supplemental Fig. S32A). Although in contrast to *Arabidopsis*, they were exclusively in sense to the *5S rDNA* loci and showed a guanosine 5′-nucleotide (5′G) bias (>75%; not known to be preferentially loaded by any of the *Arabidopsis* AGOs) (Supplemental Fig. S32D), instead of the RdDM effector AGO4 characteristic 5′A signature seen in *Arabidopsis* (Mi et al. 2008; Havecker et al. 2010; Jullien et al. 2020).

Hence, lack of DNA methylation and H3K9me2 in *Spirodela* not only impacts degenerated and short TEs, but also impacts other RdDM targets such as *5S rDNA* repeats and further strengthens the hypothesis that such silencing mechanisms only apply to long, complete TEs. Indeed, increased H3K9me2 and DNA methylation at long TEs hints that their self-reinforcement is focused at potentially functional or recently active ones to ensure their silencing.

Long, complete TEs show signatures of RdDM activity

To gain further insights into the epigenetic patterns on long TEs, we focused on the complete LTR-RTEs of the *Copia* (RLC) and *Gypsy* (RLG) superfamilies, in which H3K9me2 levels were higher than those of H3K9me1. However, the patterns differed depending on the TE superfamily. Although in RLCs had more H3K9me2 toward the center of the TE, the same modification peaked on the edges of RLGs (Fig. 6A). Such patterns resembled those found in *Arabidopsis* intact LTR-RTEs, (Supplemental Fig. S33A). DNA methylation at CG and CHG followed a similar trend as H3K9me2 in both cases (Fig. 6B), although mCHG was comparatively lower (Fig. 6B; Supplemental Fig. S33B). Furthermore, albeit very low, peaks of mCHH were also observable at RLGs edges (Fig. 6B). Hence, the layout of epigenetic silencing marks along complete TEs in *Spirodela* is very similar to those in *Arabidopsis*.

Given that in *Arabidopsis* these patterns are partially determined by RdDM (Stroud et al. 2013; Zemach et al. 2013; Stroud et al. 2014), we inspected if sRNA mapped to complete TEs in *Spirodela*. Indeed, siRNAs derived from regions with DNA methylation and H3K9me2 were present in *Spirodela*, specifically 24 nt siRNAs, despite at lower levels than in *Arabidopsis* (Fig. 6C; Supplemental Fig. S33C). Moreover, in contrast to *5S rDNA* siRNAs, 24 nt siRNAs mapping to complete TEs displayed an increased 5′A bias, characteristic of sRNAs loaded into AGO4 (Fig. 6D), although not as preferential as in *Arabidopsis* (Supplemental Fig. S33D). Complementarity of siRNAs with DNA methylation and H3K9me2 within the TE body and/or their LTRs was validated for individual complete TEs (Fig. 6E–G; Supplemental Fig. S34).

To assess if TE-derived siRNAs might participate in RdDM in *Spirodela*, also given the unconventional 5′G bias of *5S rDNA* 24 nt siRNAs, we tested if its AGO4 (SpAGO4) has the same sRNA loading preference as *Arabidopsis* AGO4 (AtAGO4). To do so, we cloned genomic *AGO4* loci from both species with a Flag-HA tag for heterologous transient expression in *Nicotiana benthamiana* leaves. No Sp*AGO4* protein was detectable owing to intron retention events when expressed in *N. benthamiana* (Supplemental Fig. S35A–C). This was likely because of the inability of dicots (*N. benthamiana*) to properly process introns of the monocots (*Spirodela*) (Keith and Chua 1986; Goodall and Filipowicz 1991; Lou et al. 1993). To circumvent this limitation, we amplified and cloned full-length cDNA from one of the two *Spirodela* AGO4, *AGO4a*, and expressed it in *N. benthamiana* leaves (Supplemental Fig. S35C,D). To examine their sRNA loading preferences, AtAGO4 and SpAGO4a were immunoprecipitated (IP) from *N. benthamiana* leaf lysates (Fig. 7A; Jullien et al. 2020) and sRNAs extracted and sequenced. Like AtAGO4, SpAGO4a displayed a strong preference for 5′A 24-nt-long siRNA and reduced affinity for 21 nt siRNA, compared with the population of siRNAs present in *N. benthamiana* leaves (Fig. 7B,C).

Therefore, sRNAs might be indeed involved in maintaining DNA methylation and H3K9me2 in *Spirodela* at long complete TEs through canonical RdDM. Our analysis of silencing pathways and epigenetic patterns on TEs shows that core components required for RdDM are present in the *Spirodela* genome and, although poorly expressed, probably active during vegetative clonal propagation to silence long TEs.

Transcriptionally active TEs are source of 21/22 nt-siRNAs in *Spirodela*

We also detected the presence of very low amounts of 21–22 nt siRNAs at the edges of complete TEs (Fig. 6C). In some instances, 24 nt siRNAs overlapped with equally abundant 21–22 nt siRNAs, especially at the flanking LTR sequences (Fig. 6G; Supplemental Fig. S36). The 21–22 nt siRNAs can arise from TE edges in *Arabidopsis* (Supplemental Fig. S33C), as a result of DCL2/4 processing of Pol IV transcripts, and direct DNA methylation (Nuthikattu et al. 2013; McCue et al. 2015; Panda et al. 2020; Sigman et al. 2021). It is unlikely that the observed TE-derived 21–22 nt siRNAs participate in RdDM, owing to the low affinity of SpAGO4 to bind such siRNA sizes (Fig. 7B), and those mapping to TEs have less 5′A bias but more 5′U (Fig. 6D), a signature of AGO1-loaded sRNAs (Mi et al. 2008; Havecker et al. 2010). This hints to a potential role rather in post-transcriptional silencing (PTGS). During PTGS, 21–22 nt siRNAs loaded into AGO proteins of the AGO1/5/10/18 and AGO2/7 clades target Pol II transcripts to guide mRNA cleavage or translational repression (for review, see Fang and Qi 2016). Coincidentally, we observed expression of TEs producing 21–22 nt siRNAs in our transcriptome data sets, including, in some instances, full-length transcripts in the long-read cDNA sequencing Iso-Seq data (Fig. 6G; Supplemental Fig. S35).

Although PTGS is a well-documented control mechanism against transcriptionally active TEs in *Arabidopsis* (Slotkin et al. 2009; Teixeira et al. 2009; Marí-Ordóñez et al. 2013; Creasey

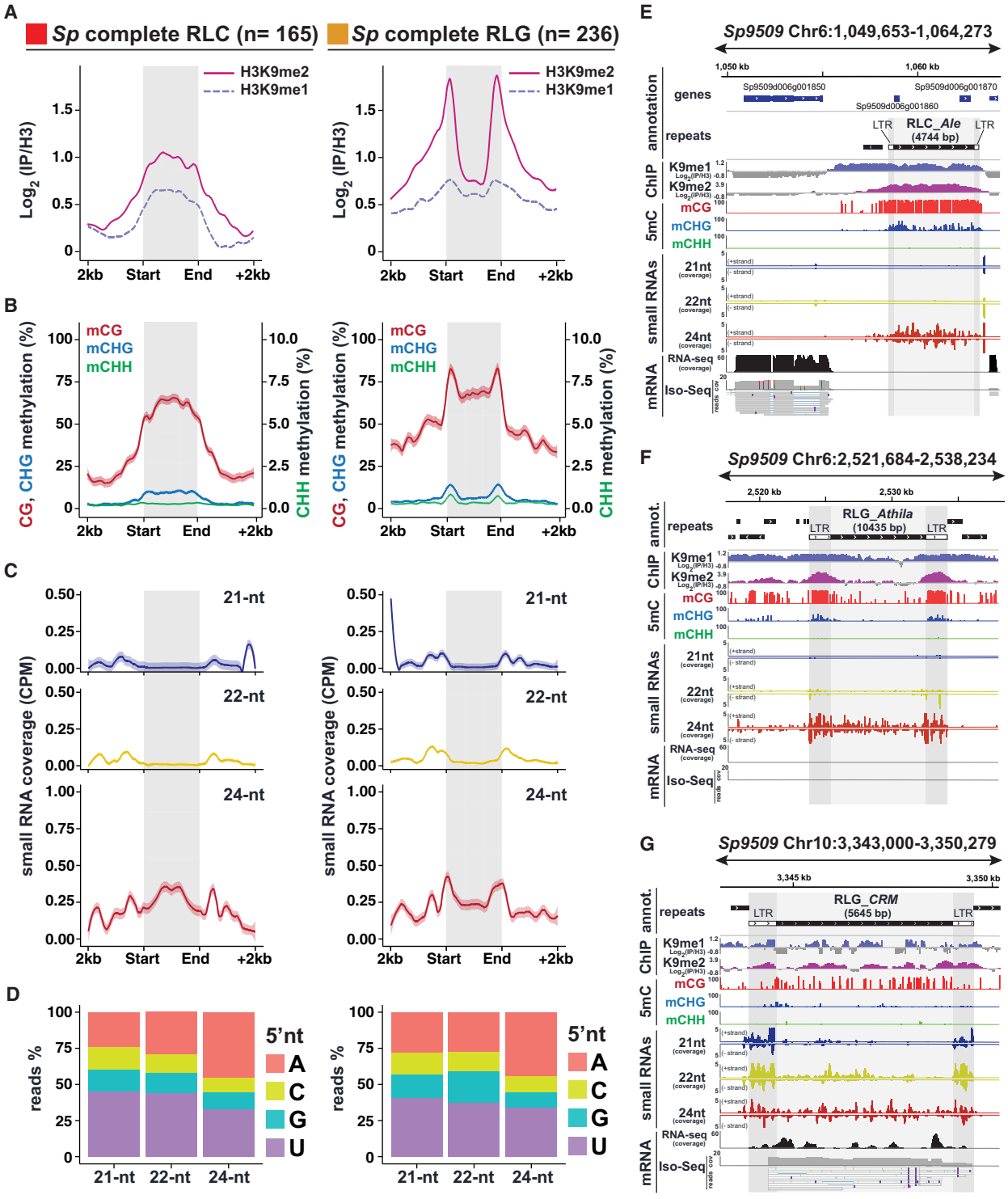

Figure 6. RdDM signatures in *S. polyrhiza* complete TEs. (*A*) Metaplots of average weighted H3K9me1 (solid line) and H3K9me2 (dashed line) enrichments over H3 at complete RLC (*left*) and RLG (*right*) transposon annotations ± 2 kb in *Spirodela*. Complete TEs were defined as those for which all RLC and RLG protein domains were identified. *n* indicates number of complete elements in each superfamily. (*B*) Metaplots of averaged weighted DNA methylation in all three contexts over RLC and RLG transposons ± 2 kb flanking regions in *Spirodela*. mCHH values are scaled to 10% max values instead of 100%. (*C*) Metaplots of averaged weighted 21, 22, and 24 nt sRNA abundance over intact RLC and RLG ± 2 kb flanking regions in *Spirodela*. In all metaplots (*A*–*D*), solid lines represent the mean, and colored shadows the SE. (*D*) 5′-Nucleotide (5′nt) composition distribution (as percentage of reads) of 21, 22, and 24 nt siRNAs mapping to intact RLC and RLG ± 2 kb flanking regions in *Spirodela*. (*E*–*G*) Genome browser captures of selected complete TEs in *Spirodela*. From *top* to *bottom*, tracks display gene and TE annotations; H3K9me1 and H3K9me2 enrichment profiles; mCG, mCHG, and mCHH methylation; 21, 22, and 24 nt siRNA mapping to Watson (+) and Crick (−) DNA strands; and RNA expression by short (Illumina) and long reads (Iso-Seq). Superfamily, clade, and length (in base pairs) of TEs is indicated *above* their annotation. Light and dark gray shadow delimit TEs and LTRs, respectively, across all tracks.

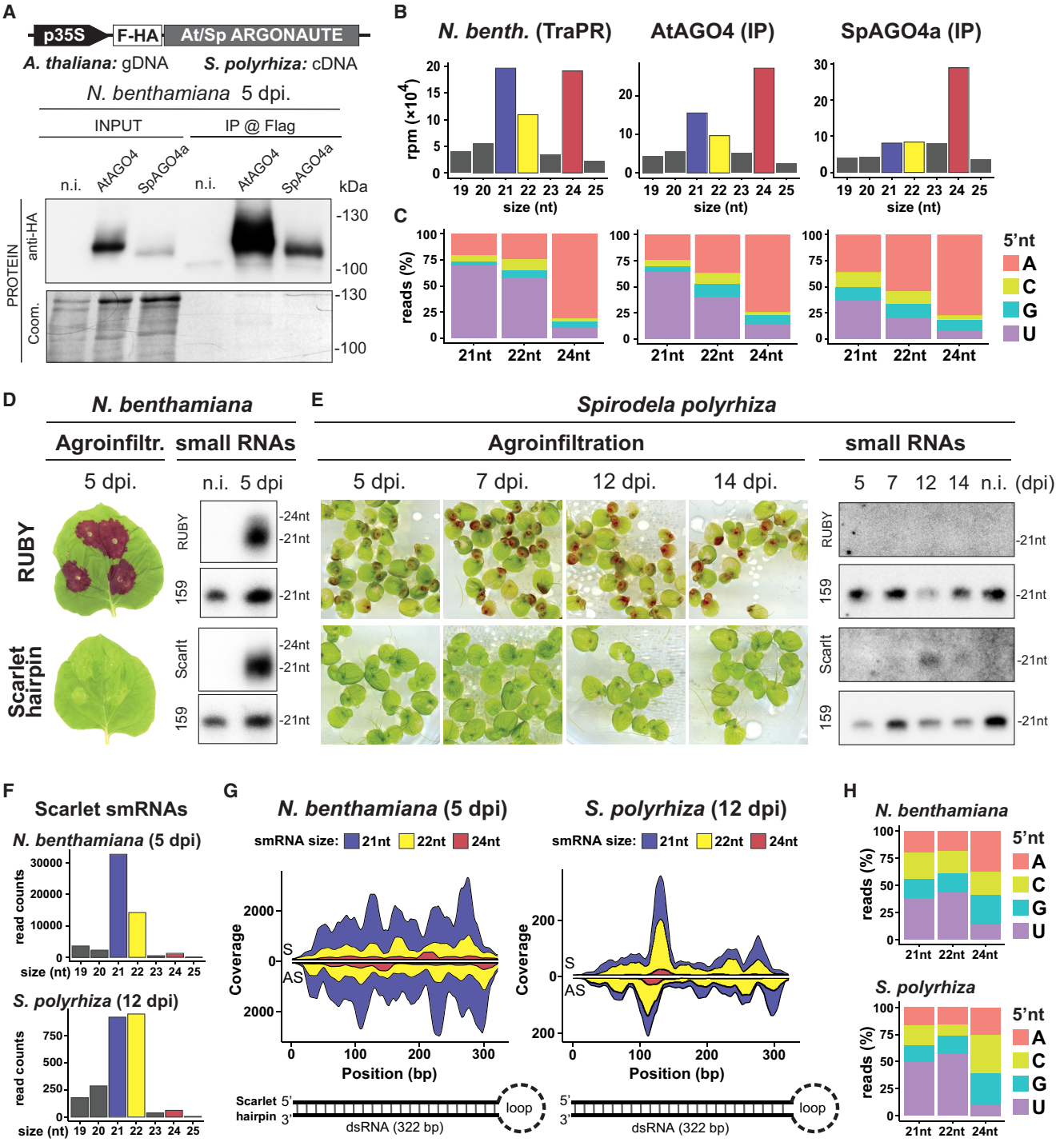

Figure 7. *S. polyrhiza* AGO4a siRNA loading preferences and IR-derived siRNAs in transient expression. (*A*) Protein blot analysis of *Arabidopsis* and *Spirodela* AGO4 (AtAGO4 and SpAGO4a) input and IP fractions from transient expression in *N. benthamiana* 5 days postinfiltration (dpi). (n.i.) Noninfiltrated. Coomassie (Coom.) staining of blot is shown as control for input and IP fractions. Scheme of constructs infiltrated in *N. benthamiana* leaves for transient expression is shown above. (p35S) CaMV 35S promoter, (F-HA) in-frame N-term Flag and HA peptide tags. Genomic DNA (gDNA) or cDNA origin of the AGO4 sequences is indicated. (*B*) Size distribution and abundance in reads per million (rpm) of TraPR purified *N. benthamiana* siRNAs (as control) and siRNAs extracted from AtAGO4 and spAGO4a IPs. (*C*) 5′-Nucleotide (5′nt) composition distribution (as percentage of reads) of 21, 22, and 24 nt siRNAs from *B*. (*D*) Representative pictures of *N. benthamiana* leaves agroinfiltrated for transient expression of RUBY or the scarlet hairpin (*hpScarlet*) IR next to sRNA blot analysis in noninfiltrated and 5 dpi leaves. miRNA159 is shown as loading control. (*E*) Representative pictures of *Spirodela* fronds agroinfiltrated for transient expression of *RUBY* or *hpScarlet* and sRNA blot analysis in noninfiltrated and infiltrated samples at different time points. miRNA159 as loading control. (*F*) Size distribution and abundance of sRNAs mapping to *hpScarlet* from 5 dpi *N. benthamiana* and 12 dpi *Spirodela*. (*G*) Stacked distribution of sense (S) and antisense (AS) sRNA coverage by size along *hpScarlet* hairpin in *N. benthamiana* and *Spirodela*. Schematic representation of the IR is depicted *below*. (*H*) 5′-nucleotide (5′nt) composition distribution of 21, 22, and 24 nt siRNAs mapping to *hpScarlet* in *N. benthamiana* and *Spirodela*.

et al. 2014; Lee et al. 2020; Oberlin et al. 2022), the potential role of 21–22 nt siRNAs in TE silencing in *Spirodela* remains to be experimentally tested.

The 22 nt siRNAs are produced in *Spirodela* despite the lack of a DCL2 ortholog

We were intrigued by the presence of TE-derived 22 nt siRNAs, given that any identifiable ortholog of DCL2, their cognate Dicer in plants (Xie et al. 2005; Henderson et al. 2006; Wang et al. 2018; Jia et al. 2020), is missing in *Spirodela* and duckweed genomes in general (Fig. 2B; Supplemental Fig. S8; Ernst et al. 2023; Harkess et al. 2024).

Their co-occurrence with 21 nt siRNAs, (Fig. 6G; Supplemental Fig. S35) suggested a common RNA substrate. Given the low amounts of 21-22 nt siRNAs mapping to individual TEs, to rule out artifacts and inspect if other endogenous siRNA sources are as well processed into 22 nt siRNAs, we investigated *Spirodela trans*-acting siRNAs (tasiRNAs). In *Arabidopsis*, tasiRNAs are processed from transcripts of specific loci (TASs), mainly into 21 nt-siRNA by DCL4 to, through their association with AGO1, regulate several target mRNAs by PTGS (Yoshikawa et al. 2005). As the TAS3 locus had been previously identified in *Spirodela* (Michael et al. 2017), we scored for TAS3 matching siRNAs in our TraPR data sets. In contrast to *Arabidopsis*, in which TAS3 tasiRNAs are almost exclusively 21 nt long, in *Spirodela*, TAS3 tasiRNAs were found as 21 and 22 nt, the latter accounting for about one-third of TAS3 tasiRNAs (Supplemental Fig. S37A,B). Their 5′U bias also suggest their preferential loading into AGO1 (Supplemental Fig. S37C).

Next, to independently test if *Spirodela* can produce 22 nt siRNAs in the absence of DCL2, we attempted to stimulate sRNA biogenesis through expression of suitable exogenous substrate RNAs. As stable transformation in *Spirodela* is difficult, we chose *Agrobacterium*-mediated transient expression. This technique has been widely used to trigger and investigate silencing mechanisms, owing to the quick onset of siRNA production in response to expression of double-stranded RNA (dsRNA) following infiltration of plant tissue with *Agrobacterium* carrying the corresponding transgenes (Hamilton et al. 2002; Andrieu et al. 2012; Bertazzon et al. 2012; Sun et al. 2014; Jay et al. 2023). We developed a modified protocol for frond transformation in *Lemna minor* (Yang et al. 2018) and applied it successfully to induce transient transgene expression in *Spirodela* fronds (Supplemental Fig. S38). We used the visual reporter *RUBY* (He et al. 2020) and an inverted repeat (IR) derived from the coding sequence of the fluorescent reporter *Scarlet* (*Scarlet* hairpin [*hpScarlet*]) (Incarbone et al. 2023). Both constructs triggered siRNAs when infiltrated into *N. benthamiana* as expected (Fig. 7D). In *Spirodela*, however, we could not detect *RUBY*-derived siRNAs by RNA blotting even after 2 weeks after infiltration. Given transgene sense PTGS (S-PTGS) is generally associated with high levels of transgene expression, the apparent lack of S-PTGS in *Spirodela* might be because of reduced expression of the reporter compared with *N. benthamiana*. On the other hand, *hpScarlet*-derived siRNAs were observed 12- and 14-days after infiltration and were lost shortly after (Fig. 7E), likely owing to loss of transgene expression inherent to the *Agrobacterium*-mediated transient expression method. Sequencing sRNAs from both *N. benthamiana* and *Spirodela* infiltrated with *hpScarlet* showed that the IR is processed into 21–22 nt siRNAs in both plants. However, *Spirodela* produced relatively equal amounts of 21 and 22 nt siRNAs, as observed for TEs, whereas the profile in *N. benthamiana* is dominated by 21 nt siRNAs (Fig. 7F). Both siRNA sizes were distributed along the length of the IR dsRNA (Fig. 7G) and displayed the 5′U bias signature of AGO1 loading (Fig. 7H).

Hence, *Spirodela* is capable of producing 22 nt siRNAs in the absence of DCL2, supporting that 21–22 nt siRNAs mapped to TEs are bona fide siRNAs. Given the similar 21–22 nt siRNA patterns observed between TEs, miRNA-triggered secondary tasiRNAs, and IR-derived siRNAs, 21–22 nt siRNAs mapped to transcriptionally active TEs are likely the result of (1) a shared miRNA targeting event to initiate secondary siRNAs, shown to regulate some TEs in other plants (Creasey et al. 2014; Šurbanovski et al. 2016), or (2) direct processing of RNA hairpins commonly present in LTRs (Benachenhou et al. 2013).

Discussion

Based on high-resolution genomic information of a duckweed species during its clonal reproduction, we have provided a detailed analysis of TE content, the epigenetic configuration at TEs, and several components expected to contribute to the silencing pathways that control TE activity in other angiosperms. Our results reinforce the idea that, with few exceptions, the *Spirodela* genome encodes only a reduced set of both PTGS and TGS components compared with *Arabidopsis*, some of which are absent or display a reduced set of paralogs, partially accounting for its reduced levels of DNA methylation and other epigenetic marks generally associated with TEs. The unique epigenome of *Spirodela* is the result of the loss of DNA methylation, and reduced levels of H3K9me2 associated to it, in highly abundant degenerated TE remnants scattered across the genome that remain nonetheless associated to the heterochromatic marks H3K9me1 and H3K27me1. In contrast, potentially intact or recently active TEs display all the epigenetic signatures associated with silencing in angiosperms. Another interesting observation is the loss of any of the silencing marks inspected here in *5S rDNA* repeats. Although this might reflect the preferential selectivity of RdDM for long TEs, lack of silencing might as well be owing to the reduced number of *5S rDNA* repeats in *Spirodela*, compared with other angiosperms, to ensure enough 5S rRNA expression for ribosome biogenesis. These changes in epigenetic regulation and silencing might be a consequence of the simplified morphology or reduced tissue and cell types in duckweeds compared with other angiosperms (Wang et al. 2014; Michael et al. 2020; Abramson et al. 2022; Ernst et al. 2023; Ware et al. 2023). However, it could also be a consequence of their different lifestyle or propagation mode.

Spirodela displays a broad range of adaptations to their free-floating aquatic lifestyle, such as the loss of complete stomatal closure response to prevent water loss (Fang et al. 2023). Besides TE control, RdDM plays a role in the regulation of gene expression and physiological adaptation to several abiotic stresses, such as heat, drought, salinity, or low environmental humidity (Erdmann and Picard 2020; Liu and He 2020; Urquiaga et al. 2021). Given that water supply is not limiting in aquatic environments and their higher stability to fluctuations in these parameters compared with terrestrial ones, RdDM activity in adult somatic tissues to respond to stress might have become less relevant in *Spirodela*.

Alternatively, but not mutually exclusive, the epigenetic landscape in the *Spirodela* genome might be a consequence of its reproduction strategy. Asexual reproduction has been linked to lower TE activity and content as TEs require sexual reproduction to spread horizontally within populations. In absence of sexual reproduction, TEs may instead become locked in vertical clonal lineages. Additionally, they might go extinct if their proliferation

becomes detrimental for the host without increased purifying selection of new TE insertions facilitated by sex (Arkhipova and Meselson 2000; Wright and Finnegan 2001; Bast et al. 2019; Dechaud et al. 2019). Furthermore, RdDM activity over short TE remnants, leading to the production of 24 nt siRNAs, is seen as an immunity memory against mobilization or invasion by related intact TEs (Nguyen and Gutzat 2022), akin to the piRNA pathway in animals (Czech et al. 2018). Thus, TEs potentially being less active during *Spirodela* clonal propagation might have led to the loss of DNA methylation, RdDM expression, and lack of components required for its activity during vegetative development such as SHH1 and CLSY1/2 (Zhou et al. 2022) over TE fragments. Maintenance of heterochromatin at such repetitive TEs remnants through H3K9me1 and H3K27me1 independently of DNA methylation might ensure proper chromatin organization and stability, preventing TE interference with transcriptional and RNA processes (Kim and Zilberman 2014; Huff et al. 2016; Sammarco et al. 2022; Ilık et al. 2024), illegitimate recombination, or rereplication of repeats during cell division (Jacob et al. 2009; Chénais et al. 2012; Stroud et al. 2012; Bourque et al. 2018; Dong et al. 2021). The presence of dense TE clusters marked by H3K27me3 might also prevent genome instability as their alternative regulation by DNA and H3K9 methylation could mimic centromeric and pericentromeric regions, leading to the formation of polycentromeric chromosomes highly unstable during mitosis (Fu et al. 2012). As inactivation of secondary centromeres has been linked to increased H3K27me2/3 in wheat (Zhang et al. 2010), such TE-rich clusters might correspond to inactive centromeres in *Spirodela*. Deeper characterization of the chromatin structure (e.g., chromatin accessibility) and landscape (e.g., additional histone modifications, histone variants), together with functional studies, might shed light onto the regulation of H3K9me1, H3K27me1, H3K27me3, and their role in shaping heterochromatin, TE silencing, and genome stability regulation in *Spirodela* and other plants.

Furthermore, unlike vegetative propagation in other plants in which clones originate from differentiated organs such as stems, roots, or leaves, with tissue-specific and developmentally regulated TEs, new individuals in duckweeds originate from a dedicated group of stem cells (Landolt 1986). This might have further favored a relaxation of epigenetic and RdDM-mediated TE control in somatic tissues that do not participate in vegetative reproduction in *Spirodela*. Nevertheless, potentially intact TEs are under several layers of epigenetic control, including RdDM, suggesting the pathway might be tissue specific or developmentally regulated.

In contrast to stem cells in other angiosperms contained in a well-organized shoot apical meristem (SAM) that generates new organs (Gaillochet and Lohmann 2015), meristems in *Spirodela* and all duckweeds are formed by unstructured groups of few undifferentiated cells, which generate new meristems that develop into DFs. (Landolt 1986; Lemon and Posluszny 2000; Sree et al. 2015; Yang et al. 2021; Li et al. 2023a). To maintain genome integrity along the clonal lineage, RdDM might be expressed in the few stem cells within the budding pockets or during the developmental window between the formation of a new meristem and its development into a new frond with its own stem cells.

Furthermore, lack of or weakened RdDM activity owing to losses such as DRM3, CLSY1, SHH1, and absence of CMT2, in combination with weak CMT3/ZMET activity in somatic tissues during development, will suffice to explain the global loss of mCHH and low levels of mCHG. Additionally, the higher variation in mCG levels in *Spirodela* could be a consequence of mCG maintenance being less efficient or not active in all cells or of not all CG sites being as faithfully maintained. Altogether, this might, in some instances, permit transcription of some TEs that then trigger 21–22 nt siRNAs. Alternatively, transient relaxation of TE control and TE expression has been shown to take place in *Arabidopsis* meristematic stem cells during developmental transitions (Gutzat et al. 2020). A similar phenomenon taking place during the development of new meristems and fronds might as well explain the paradox of observed expression from TEs covered in silencing marks and the apparent simultaneous presence of sRNAs associated with TGS and PTGS. Further tissue- and cell-specific investigation of epigenetic parameters will be able to address these hypotheses.

Nonetheless, although infrequent, *Spirodela* does flower occasionally (Fourounjian et al. 2021), and its population genetic structure shows signs of sexual reproduction (Ho et al. 2019; Wang et al. 2024). Hence, RdDM might still be relevant and active during sexual reproduction as suggested by the presence of CLSY3, which recruits RdDM to TEs during flowering in *Arabidopsis* (Long et al. 2021; Zhou et al. 2022). Nonetheless, we note that the function of silencing components present and absent in *Spirodela* might play different roles in duckweeds (and other monocots) compared with those described in *Arabidopsis* given their evolutionary distance. Hence, a full understanding of TE silencing in duckweeds will require further molecular genetics and biochemical characterization of their silencing pathways.

Adding to the unique epigenetic regulation of degenerated TEs and their relics in *Spirodela* here described, one of the intriguing results of our study is the constatation that, despite lack of DCL2, *Spirodela* can produce 22 nt siRNAs, nearly as abundantly loaded in AGOs as 21 nt siRNAs, not only from TEs but also from endogenous and exogenous sources of dsRNA. As these sources of siRNAs are generally products of DCL4 in plants (Xie et al. 2005; Fusaro et al. 2006; Parent et al. 2015), given the overlap between 22 and 21 nt but not 24 nt (DCL3), we consider processing dsRNA into 22 nt siRNAs by *Spirodela* DCL4 as a plausible explanation. Alternatively, DCL3 in *Arabidopsis* has been shown to be able to process certain dsRNA precursors into 22 nt siRNAs in vitro (Loffer et al. 2022) and is responsible for 22–24 nt siRNA biogenesis in the moss *Physcomitrium patens* (Cho et al. 2008). Therefore, *Spirodela* DCL3 might as well be responsible for the biogenesis of 22 nt siRNAs in *Spirodela*. Future genetic and biochemical characterization of *Spirodela* DCLs will be required to understand the factors responsible for the biogenesis of 22 nt siRNAs and their role in *Spirodela* and other duckweeds. In *Arabidopsis*, DCL2 and its capacity to process dsRNA into 22 nt siRNAs have been proposed to play a dual role in antiviral immunity. On one hand, its processing of viral dsRNA acts as an innate immunity sensor (Nielsen et al. 2023, 2024). On the other hand, 22 nt siRNAs in plants guide the recruitment of RDRs to boost siRNAs production from their targets and amplify silencing (Chen et al. 2010; Zhang et al. 2012; Taochy et al. 2017; Chen et al. 2018). Their presence in *Spirodela* independently of DCL2 and the lack of several other RNAi factors associated with antiviral defense in angiosperms, as well as the apparent lack of sense transgene silencing (S-PTGS) triggered by transient expression of the *RUBY* reporter, raise several intriguing questions about RNA-based defense mechanisms in duckweeds that deserve further investigation in the future.

Hence, *Spirodela* might represent a unique model to investigate not only transposon dynamics and the epigenetic and genetic consequences of long periods of asexual reproduction but also noncanonical PTGS pathways.

Methods

Spirodela culture and growth conditions

Spirodela polyrhiza

Spirodela was grown on half-strength Schenk and Hildebrandt (½ SH, Duchefa Biochemie S0225) liquid medium in Magenta GA-7 containers (Sigma-Aldrich V8505), culture dishes (Greiner Bio-One 664160), six-well culture plates (Greiner Bio-One 657185), or in 1 L glass beakers (covered with a sterile plastic lid), all sealed with Leucopore tape (Duchefa Biochemie L3301), under long-day conditions (16-h light/8-h dark) at 21°C with a light intensity of 85 $\mu M/m^2/s^1$. The *S. polyrhiza* 9509 clone was obtained from the Landolt collection, recently transferred to the CNR-IBBA_MIDW collection (Morello et al. 2024; https://biomemory.cnr.it/collections/CNR-IBBA-MIDW).

Further information regarding *Spirodela* sterilization for axenic cultures and long-term storage, *Arabidopsis* and *N. benthamiana* material information and culture and plant imaging can be found within the Supplemental Methods in the Supplemental Material.

Genome sequencing and gene annotation

Genomic DNA from *Spirodela* was purified using the Dneasy Plant mini kit (Qiagen 69104) following the manufacturer's instructions. Library preparation was carried using the NEBNext Ultra II DNA library prep kit for Illumina (NEB E7103). Sequencing was performed on an Illumina HiSeq4A to produce paired-end reads of 125 bp. The Landolt Sp9505 genome was generated by pseudoassembly with MaSuRCA (version 3.4.1, default parameters) (Zimin et al. 2013), using as scaffold the Sp9509_Oxforrd_v3 reference assembly (Hoang et al. 2018). The pseudoassembly was polished using POLCA (Zimin and Salzberg 2020). Variation, between the two assemblies, was further evaluated using GAKT (version 4.0.1.2) (McKenna et al. 2010), in particular with HaplotypeCaller (--standard-min-confidence-threshold-for-calling 30) (Poplin et al. 2018). Variants identified were summarized into a table using GAKT VariantsToTable (-F CHROM -F POS -F TYPE -GF AD). Gene annotations were transferred from the latest annotated version of Sp9509 (Ernst et al. 2023) obtained from https://www.lemna.org. Annotation transfer was performed using Liftoff (version 1.6.3) (Shumate and Salzberg 2021) using default parameters. Information regarding the phylogenetic analysis and protein domain annotations of *Spirodela* silencing components can be found within the Supplemental Methods in the Supplemental Material.

Transposon annotation

The annotation of TEs in *S. polyrhiza* was performed by combining EDTA (Ou et al. 2019) and RepeatModeler2 (Flynn et al. 2020) tools. To ensure accuracy, both tools were run in triplicate, and the resulting annotation libraries were aligned and merged. The classification of TEs was further refined using DeepTE (-sp P) (Yan et al. 2020). The presence of the protein domain for LTR-RT was evaluated using TEsorter (version 1.3, -db rexdb-plant -st nucl) (Zhang et al. 2022).

Transcriptome analysis

To extract RNA from *Spirodela*, 100 mg of plant material was flash-frozen upon harvesting and ground. The samples were homogenized in 1 mL of TRIzol (Thermo Fisher Scientific 15596018) using Silamat S6 (Ivoclar Vivadent). RNA was extracted according to the manufacturer's instructions. RNA library preparation was performed using the NEBNext Ultra II RNA library prep kit for Illumina (NEB E7775) or the SMRTbell prep kit 3.0 for Illumina and Iso-Seq, respectively. Illumina sequencing was performed on HiSeq5A to generate 125 bp paired-end reads. Long-read sequencing was performed on PacBio Sequel II. For Illumina data, base calls were performed using bcl2FASTQ (v2.17). RNA-seq reads were trimmed using Trim Galore! (v0.6, --illumina -phred33 -stringency 1 --FASTQc --length 20). Trimmed reads were mapped using HISAT2 (v2.1.0). Gene and TE expression levels were quantified separately using kallisto (v0.46) (Bray et al. 2016) with default parameters. The resulting expression levels (measured in TPM) were then averaged across the three replicates. For *Arabidopsis* seedlings, data were obtained from GSM6892967, GSM6892968, and GSM6892969 (Li et al. 2023b). Iso-Seq long reads were processed using nf-core/isoseq (https://github.com/nf-core/isoseq/tree/1.0.0). High-quality transcripts were then mapped to *Spirodela* genome using minimap2 (v2.17, default parameters) (Li 2021).

DNA methylation analysis

For EMseq, DNA extraction was performed as above. Libraries were prepared using the NEBNext EM-seq kit (NEB M7634) following the manufacturer's instructions. Sequencing was performed on an Illumina NovaSeq SP to produce paired-end reads of 150 bp. Briefly, base calls were performed using bcl2FASTQ (v2.17), and sequenced reads were quality-filtered and adaptor-trimmed using Trim Galore! version 0.6.2 (https://github.com/FelixKrueger/TrimGalore). Enzymatic-converted reads were aligned either to the TAIR10 genome or *S. polyrhiza* genome using Bismark version 0.22.2 with *Bismark* (--non_directional *-q* --score-min *L,0,–0.4*) (Krueger and Andrews 2011) to generate coverage files per cytosine. Conversion rates were assessed by mapping (with SAMtools v1.9) the reads to the unmethylated lambda phage DNA, with the same parameters used for the genome BAM files containing clonal deduplicated lineages, and uniquely mapped reads were then used to extract weighted methylation rates at each cytosine as previously described (Schultz et al. 2015). Replicates were merged into a single bedFile using the BEDTools (Quinlan and Hall 2010) merge function and only cytosines with coverage of four or greater were considered for further analyses. 5mC was calculated using ViewBS (v0.1.11) (Huang et al. 2018; https://github.com/xie186/ViewBS) using default parameters.

sRNA library preparation and analysis

The libraries were prepared according to the method of Hayashi et al. (2016). In summary, sRNAs purified from plant tissues or immunoprecipitated AGO (Supplemental Methods in Supplemental Material), using TraPR (Grentzinger et al. 2020), or from total sRNA, as described in Supplemental Methods (Supplemental Material), were ligated to 3′ barcoded DNA adapters using truncated T4 RNA ligase 2 (New England Biolabs M0373). These fragments were separated in an 12% denaturing polyacrylamide-urea gel, excised, and purified using the ZR small-RNA PAGE Recovery Kit (Zymo Research R1070). The elution was then ligated to 5′ barcoded RNA adapters using T4 RNA ligase 1 (New England Biolabs M0204). To reduce ligation biases, the sequence of both adaptors included four random nucleotides at the ends. The resulting fragments were reverse-transcribed and amplified by PCR using primers compatible with the Illumina Platform. The size distribution of the libraries was assessed using the 5200 fragment analyzer system (Agilent M5310AA). Sequencing was performed on an Illumina NextSeq550 to produce single-end reads of 75 bp. Base calls were performed using bcl2FASTQ (v2.17). Reads were trimmed and quality-checked using Trimmomatic (v0.39) (Bolger et al. 2014). Trimmed reads were mapped to *Arabidopsis* TAIR10 and *Spirodela*

genomes, as well as *RUBY* or *hpScarlet* sequences using Bowtie 2 (v1.2.2; -e 50 -a -v 0 --best --strata --nomaqround -y --phred33-quals --no-unal --sam) (Langmead and Salzberg 2012). Mapped reads were then normalized using bamCoverage (DeepTools v, --normalizeUsing CPM --binSize 1 --smoothLength 10 --maxFragmentLength 30) (Ramírez et al. 2016). To visualize strand, mapped reads were split using SAMtools view (SAMtools v1.9, using -h -b -F 16 or -h -b -f 16 options) (Li et al. 2009).

Chromatin immunoprecipitation

ChIP was conducted on 2 g of *Arabidopsis* 10-day-old seedlings (WT Col-0) and *S. polyrhiza* 9509 fronds. Following standard procedures (for detailed method, see Supplemental Methods in Supplemental Material) using the following antibodies: anti-H3 (rabbit polyclonal, Abcam ab1791), anti-H3K27me3 (rabbit polyclonal, Merck-Millipore 07–449), anti-H3K4me3 (rabbit polyclonal, Abcam ab8580), anti-H3K9me1 (rabbit polyclonal, Abcam 3ab8896), anti-H3K9me2 (mouse monoclonal, Abcam ab1220), or anti-H3K27me1 (rabbit polyclonal, Merck-Millipore 17–643). Further detailed information on ChIP sample preparation and histone PTM procedures and analysis by mass spectrometry can be found within the Supplemental Methods in the Supplemental Material.

ChIP-seq library prep and data processing

For ChIP-seq, libraries were prepared using the NEBNext Ultra II DNA library prep kit for Illumina (NEB E7103) according to the manufacturer's instructions. Sequencing was performed on an Illumina NovaSeq S4 to produce paired-end reads of 150 bp. The raw BAM files were converted to FASTQ using BEDTools (v2.27.1, default parameters) (Quinlan and Hall 2010) for quality assessment of the sequenced samples. FASTQc (v0.11.8, default parameters; https://www.bioinformatics.babraham.ac.uk/projects/fastqc/) was used to generate quality reports for all sequencing data. Base calls were performed using bcl2FASTQ (v2.17). Trimming of reads was performed using trim_galore (v0.6.5, --dont_gzip --stringency 1 --fastqc --length 5′; https://zenodo.org/doi/10.5281/zenodo.5127898). The aligned reads were then mapped to either the TAIR10 *Arabidopsis* genome or *S. polyrhiza* genome using Bowtie 2 (v2.4.1, default parameters) (Langmead and Salzberg 2012). Duplicate reads were removed using Picard (v2.22.8, default parameters; http://broadinstitute.github.io/picard/). Mapped reads were then normalized using bam Coverage (deepTools v3.3.1). Correlations between ChIP samples were evaluated using deepTools (v3.1.2, default parameters) (Ramírez et al. 2016). The bamCompare function from deep Tools was used to normalize ChIP samples to Input or H3 and produce $\log_2$ ratio (ChIP/H3) bigWig files. Peak calling was performed using MACS2 (v2.2.5 –nomodel –nolambda –broad -q 0.01 -f BAMPE -g 138550563) (Zhang et al. 2008).

Plasmids used in this study

All plasmids generated have been submitted to Addgene (www.addgene.org) and can be retrieved under the following IDs: p*35S:FHA*-At*AGO4*_gDNA (216838), p*35S:FHA*-Sp*AGO4a*_gDNA (216841), and p*35S*::*FHA*-Sp*AGO4a*_cDNA (216842). The following plasmids previously originated in work by He et al. (2020) and Oberlin et al. (2017) were obtained from Addgene: p*35S:RUBY* (160908), p*ZmUbq:RUBY* (160909), and p*35S:GFP-GUS* (167122). p3At*UBQ:hpScarlet* was a gift from Marco Incarbone (Max-Planck-Institute of Plant Physiology). Cloning and transient expression procedures in both *Spirodela* and Tobacco can be found in the Supplemental Methods (Supplemental Material). Primers used for cloning can be found in Supplemental Figure S39.

sRNA and protein blotting

RNA and protein gels, blotting, and detection were performed using standard procedures detailed in the Supplemental Methods (Supplemental Material) together with probes (Supplemental Fig. S39) and antibodies used in this study.

Staining of nuclei

DAPI-staining of interphase nuclei was performed as described in the Supplemental Methods (Supplemental Material).

Visualization and statistical analysis

Data visualization files were generated according to each specific sections. Statistical tests were performed using R-dependent ggpubr (v0.6.0; https://rpkgs.datanovia.com/ggpubr/); the statistical tests performed are indicated accordingly on each figure legend figure. Plots under R (v4.2.2; https://www.r-project.org) were generated using *circlize* (v0.4.15) (Gu et al. 2014), ggplot2 (v3.4.4) (Wickham 2009), profileplyr (v1.14.1; https://bioconductor.org/packages/release/bioc/html/profileplyr.html), ViewBS (v0.1.11) (Huang et al. 2018), or pheatmap (v 1.0.12; https://rdocumentation.org/packages/pheatmap/versions/1.0.12).

Raw data and source files

An inventory of all the raw data used to generate each figure panel (as well as those in Supplemental Information) along with all raw image files (including RNA, protein blots, and agarose gels), DNA and protein sequences, alignments, and phylogenetic tree files can be found in Supplemental Material, as well as in Zenodo (https://doi.org/10.5281/zenodo.14037413). Additionally, ready-to-use Integrative Genomics Viewer (IGV) genome browser tracks for all the sequencing data sets generated here are available in the associated Zenodo data set.

Data access

All the sequencing data generated for this study have been submitted to the NCBI BioProject database (https://www.ncbi.nlm.nih.gov/bioproject/) under accession number PRJNA1164696. The mass spectrometry proteomics data have been deposited to the ProteomeXchange Consortium via the PRIDE partner repository (https://www.ebi.ac.uk/pride/) with the data set identifier PXD050443.

Competing interest statement

The authors declare no competing interests.

Acknowledgments

This work was supported by the Gregor Mendel Institute of Plant Molecular Biology (GMI) of the Austrian Academy of Sciences (ÖAW) core funding attributed to A.M.-O. We thank current and past members of the Marí-Ordóñez group and colleagues from the Gregor Mendel Institute and the Vienna BioCenter (VBC) campus for fruitful discussions, ideas, and feedback. We also thank Klaus Appenroth from the Friedrich Schiller University of Jena for useful advice on duckweed cultivation and storage, Thomas Grentzinger for technical assistance with the TraPR procedure, and Marco Incarbone from the Max-Planck-Institute of Plant

Physiology in Golm for kindly providing the pAt*UBQ:hpScarlet* plasmid. We thank the Vienna BioCenter Core Facilities (VBCF): NGS for DNA, EM-seq, PacBio, RNA-seq and ChIP-seq library preparation and sequencing, including sequencing of sRNA libraries; the IMP/IMBA/GMI Proteomics Facility, especially Ines Steinmacher for sample preparation, mass spectrometry using the VBCF instrument pool, and Richard Imre and Elisabeth Rothinger for assistance with data analysis of histone PTMs; the Plant Science Facility for assistance with plant work; and the IMP Molecular Biology Service for providing reagents and Sanger sequencing. Lastly, we thank the VBC in-house COVID-19 testing facility for enabling a safe working environment during the pandemic.

Author contributions: A.M.-O. conceived and designed the study. R.D., V.B.-B., and D.B.-A. performed most of the experiments. A.M.-O., R.D., and D.B.-A. performed identification and phylogenetic analysis of silencing components in *Spirodela*. V.B.-B. cloned and carried out transient *AGO4* expression experiments and prepared sRNA libraries. D.B.-A. made nuclei DAPI staining. J.M.V.-G. performed western blot analysis of HPTMs. A.M.-O., D.B.-A., and A.P.-M. optimized agroinfiltration-mediated transient expression in duckweeds. A.P.-M. carried out transient expression experiments in *Spirodela*. V.B.-B. and R.E. cultured and maintained *Spirodela* stocks and axenic cultures and provided technical support. R.D. and D.B.-A. performed computer and statistical analysis. A.M.-O., R.D., and D.B.-A. analyzed the data and wrote the manuscript. A.M.O., D.B.-A., and L.D.-N. addressed editorial and referee's comments and prepared the revised and final versions of the manuscript.

References

Abramson BW, Novotny M, Hartwick NT, Colt K, Aevermann BD, Scheuermann RH, Michael TP. 2022. The genome and preliminary single-nuclei transcriptome of *Lemna minuta* reveals mechanisms of invasiveness. *Plant Physiol* **188:** 879–897. doi:10.1093/plphys/kiab564

Allshire RC, Madhani HD. 2018. Ten principles of heterochromatin formation and function. *Nat Rev Mol Cell Biol* **19:** 229–244. doi:10.1038/nrm.2017.119

An D, Zhou Y, Li C, Xiao Q, Wang T, Zhang Y, Wu Y, Li Y, Chao D-Y, Messing J, et al. 2019. Plant evolution and environmental adaptation unveiled by long-read whole-genome sequencing of *Spirodela*. *Proc Natl Acad Sci* **116:** 18893–18899. doi:10.1073/pnas.1910401116

Andrieu A, Breitler JC, Siré C, Meynard D, Gantet P, Guiderdoni E. 2012. An in planta, agrobacterium-mediated transient gene expression method for inducing gene silencing in rice (*Oryza sativa* L.) leaves. *Rice* **5:** 23. doi:10.1186/1939-8433-5-23

Arkhipova I, Meselson M. 2000. Transposable elements in sexual and ancient asexual taxa. *Proc Natl Acad Sci* **97:** 14473–14477. doi:10.1073/pnas.97.26.14473

Bast J, Jaron KS, Schuseil D, Roze D, Schwander T. 2019. Asexual reproduction reduces transposable element load in experimental yeast populations. *eLife* **8:** e48548. doi:10.7554/eLife.48548

Benachenhou F, Sperber GO, Bongcam-Rudloff E, Andersson G, Boeke JD, Blomberg J. 2013. Conserved structure and inferred evolutionary history of long terminal repeats (LTRs). *Mob DNA* **4:** 5. doi:10.1186/1759-8753-4-5

Bertazzon N, Raiola A, Castiglioni C, Gardiman M, Angelini E, Borgo M, Ferrari S. 2012. Transient silencing of the grapevine gene *VvPGIP1* by agroinfiltration with a construct for RNA interference. *Plant Cell Rep* **31:** 133–143. doi:10.1007/s00299-011-1147-2

Bewick AJ, Schmitz RJ. 2017. Gene body DNA methylation in plants. *Curr Opin Plant Biol* **36:** 103–110. doi:10.1016/j.pbi.2016.12.007

Bewick AJ, Ji L, Niederhuth CE, Willing E-M, Hofmeister BT, Shi X, Wang L, Lu Z, Rohr NA, Hartwig B, et al. 2016. On the origin and evolutionary consequences of gene body DNA methylation. *Proc Natl Acad Sci* **113:** 9111–9116. doi:10.1073/pnas.1604666113

Bewick AJ, Niederhuth CE, Ji L, Rohr NA, Griffin PT, Leebens-Mack J, Schmitz RJ. 2017. The evolution of CHROMOMETHYLASES and gene body DNA methylation in plants. *Genome Biol* **18:** 65. doi:10.1186/s13059-017-1195-1

Biémont C, Vieira C. 2006. Genetics: junk DNA as an evolutionary force. *Nature* **443:** 521–524. doi:10.1038/443521a

Bies-Etheve N, Pontier D, Lahmy S, Picart C, Vega D, Cooke R, Lagrange T. 2009. RNA-directed DNA methylation requires an AGO4-interacting member of the SPT5 elongation factor family. *EMBO Rep* **10:** 649–654. doi:10.1038/embor.2009.31

Blevins T, Pontes O, Pikaard CS, Meins F Jr. 2009. Heterochromatic siRNAs and DDM1 independently silence aberrant 5S rDNA transcripts in *Arabidopsis*. *PLoS One* **4:** e5932. doi:10.1371/journal.pone.0005932

Blumenstiel JP. 2019. Birth, school, work, death, and resurrection: the life stages and dynamics of transposable element proliferation. *Genes (Basel)* **10:** 336. doi:10.3390/genes10050336

Bog M, Appenroth K-J, Sree KS. 2019. Duckweed (Lemnaceae): its molecular taxonomy. *Front Sustain Food Syst* **3:** 117. doi:10.3389/fsufs.2019.00117

Bolger AM, Lohse M, Usadel B. 2014. Trimmomatic: a flexible trimmer for Illumina sequence data. *Bioinformatics* **30:** 2114–2120. doi:10.1093/bioinformatics/btu170

Bourc'his D, Voinnet O. 2010. A small-RNA perspective on gametogenesis, fertilization, and early zygotic development. *Science* **330:** 617–622. doi:10.1126/science.1194776

Bourque G, Burns KH, Gehring M, Gorbunova V, Seluanov A, Hammell M, Imbeault M, Izsvák Z, Levin HL, Macfarlan TS, et al. 2018. Ten things you should know about transposable elements. *Genome Biol* **19:** 199. doi:10.1186/s13059-018-1577-z

Bradamante G, Nguyen VH, Incarbone M, Meir Z, Bente H, Donà M, Lettner N, Scheid OM, Gutzat R. 2024. Two ARGONAUTE proteins loaded with transposon-derived small RNAs are associated with the reproductive cell lineage in *Arabidopsis*. *Plant Cell* **36:** 863–880. doi:10.1093/plcell/koad295

Bray NL, Pimentel H, Melsted P, Pachter L. 2016. Near-optimal probabilistic RNA-seq quantification. *Nat Biotechnol* **34:** 525–527. doi:10.1038/nbt.3519

Brosseau C, Moffett P. 2015. Functional and genetic analysis identify a role for *Arabidopsis* ARGONAUTE5 in antiviral RNA silencing. *Plant Cell* **27:** 1742–1754. doi:10.1105/tpc.15.00264

Cao HX, Vu GTH, Wang W, Messing J, Schubert I. 2015. Chromatin organisation in duckweed interphase nuclei in relation to the nuclear DNA content. *Plant Biol* **17:** 120–124. doi:10.1111/plb.12194

Carbonell A, Fahlgren N, Garcia-Ruiz H, Gilbert KB, Montgomery TA, Nguyen T, Cuperus JT, Carrington JC. 2012. Functional analysis of three *Arabidopsis* ARGONAUTES using slicer-defective mutants. *Plant Cell* **24:** 3613–3629. doi:10.1105/tpc.112.099945

Cervantes-Pérez SA, Yong-Villalobos L, Florez-Zapata NMV, Oropeza-Aburto A, Rico-Reséndiz F, Amasende-Morales I, Lan T, Martínez O, Vielle-Calzada JP, Albert VA, et al. 2021. Atypical DNA methylation, sRNA-size distribution, and female gametogenesis in *Utricularia gibba*. *Sci Rep* **11:** 15725. doi:10.1038/s41598-021-95054-y

Chan SW-L, Zilberman D, Xie Z, Johansen LK, Carrington JC, Jacobsen SE. 2004. RNA silencing genes control de novo DNA methylation. *Science* **303:** 1336. doi:10.1126/science.1095989

Chen H-M, Chen L-T, Patel K, Li Y-H, Baulcombe DC, Wu S-H. 2010. 22-Nucleotide RNAs trigger secondary siRNA biogenesis in plants. *Proc Natl Acad Sci* **107:** 15269–15274. doi:10.1073/pnas.1001738107

Chen W, Zhang X, Fan Y, Li B, Ryabov E, Shi N, Zhao M, Yu Z, Qin C, Zheng Q, et al. 2018. A genetic network for systemic RNA silencing in plants. *Plant Physiol* **176:** 2700–2719. doi:10.1104/pp.17.01828

Chen G, Stepanenko A, Borisjuk N. 2021. Mosaic arrangement of the 5S rDNA in the aquatic plant *Landoltia punctata* (Lemnaceae). *Front Plant Sci* **12:** 678689. doi:10.3389/fpls.2021.678689

Chen G, Stepanenko A, Borisjuk N. 2024. Contrasting patterns of 5S rDNA repeats in European and Asian ecotypes of greater duckweed, *Spirodela polyrhiza* (Lemnaceae). *Front Plant Sci* **15:** 1378683. doi:10.3389/fpls.2024.1378683

Chénais B, Caruso A, Hiard S, Casse N. 2012. The impact of transposable elements on eukaryotic genomes: from genome size increase to genetic adaptation to stressful environments. *Gene* **509:** 7–15. doi:10.1016/j.gene.2012.07.042

Cho SH, Addo-Quaye C, Coruh C, Arif MA, Ma Z, Frank W, Axtell MJ. 2008. *Physcomitrella patens* DCL3 is required for 22–24 nt siRNA accumulation, suppression of retrotransposon-derived transcripts, and normal development. *PLoS Genet* **4:** e1000314. doi:10.1371/journal.pgen.1000314

Choi J, Lyons DB, Zilberman D. 2021. Histone H1 prevents non-CG methylation-mediated small RNA biogenesis in *Arabidopsis* heterochromatin. *eLife* **10:** e72676. doi:10.7554/eLife.72676

Cokus SJ, Feng S, Zhang X, Chen Z, Merriman B, Haudenschild CD, Pradhan S, Nelson SF, Pellegrini M, Jacobsen SE. 2008. Shotgun bisulphite sequencing of the *Arabidopsis* genome reveals DNA methylation patterning. *Nature* **452:** 215–219. doi:10.1038/nature06745

Creasey KM, Zhai J, Borges F, Ex FV, Regulski M, Meyers BC, Martienssen RA. 2014. miRNAs trigger widespread epigenetically activated siRNAs from transposons in *Arabidopsis*. *Nature* **508:** 411–415. doi:10.1038/nature13069

Czech B, Munafò M, Ciabrelli F, Eastwood EL, Fabry MH, Kneuss E, Hannon GJ. 2018. piRNA-guided genome defense: from biogenesis to silencing. *Annu Rev Genet* **52:** 131–157. doi:10.1146/annurev-genet-120417-031441

Dechaud C, Volff J-N, Schartl M, Naville M. 2019. Sex and the TEs: transposable elements in sexual development and function in animals. *Mob DNA* **10:** 42. doi:10.1186/s13100-019-0185-0

Deleris A, Gallego-Bartolome J, Bao J, Kasschau KD, Carrington JC, Voinnet O. 2006. Hierarchical action and inhibition of plant dicer-like proteins in antiviral defense. *Science* **313:** 68–71. doi:10.1126/science.1128214

Diego-Martin B, Pérez-Alemany J, Candela-Ferre J, Corbalán-Acedo A, Pereyra J, Alabadí D, Jami-Alahmadi Y, Wohlschlegel J, Gallego-Bartolomé J. 2022. The TRIPLE PHD FINGERS proteins are required for SWI/SNF complex-mediated +1 nucleosome positioning and transcription start site determination in *Arabidopsis*. *Nucleic Acids Res* **50:** 10399–10417. doi:10.1093/nar/gkac826

Ding Y, Fromm M, Avramova Z. 2012. Multiple exposures to drought "train" transcriptional responses in *Arabidopsis*. *Nat Commun* **3:** 740. doi:10.1038/ncomms1732

Dong J, LeBlanc C, Poulet A, Mermaz B, Villarino G, Webb KM, Joly V, Mendez J, Voigt P, Jacob Y. 2021. H3.1K27me1 maintains transcriptional silencing and genome stability by preventing GCN5-mediated histone acetylation. *Plant Cell* **33:** 961–979. doi:10.1093/plcell/koaa027

Duan C-G, Zhang H, Tang K, Zhu X, Qian W, Hou YJ, Wang B, Lang Z, Zhao Y, Wang X, et al. 2015. Specific but interdependent functions for *Arabidopsis* AGO4 and AGO6 in RNA-directed DNA methylation. *EMBO J* **34:** 581–592. doi:10.15252/embj.201489453

Duan C-G, Wang X, Zhang L, Xiong X, Zhang Z, Tang K, Pan L, Hsu C-C, Xu H, Tao WA, et al. 2017. A protein complex regulates RNA processing of intronic heterochromatin-containing genes in *Arabidopsis*. *Proc Natl Acad Sci* **114:** E7377–E7384. doi:10.1073/pnas.1710683114

Ebbs ML, Bender J. 2006. Locus-specific control of DNA methylation by the *Arabidopsis* SUVH5 histone methyltransferase. *Plant Cell* **18:** 1166–1176. doi:10.1105/tpc.106.041400

El-Shami M, Pontier D, Lahmy S, Braun L, Picart C, Vega D, Hakimi MA, Jacobsen SE, Cooke R, Lagrange T. 2007. Reiterated WG/GW motifs form functionally and evolutionarily conserved ARGONAUTE-binding platforms in RNAi-related components. *Genes Dev* **21:** 2539–2544. doi:10.1101/gad.451207

Erdmann RM, Picard CL. 2020. RNA-directed DNA methylation. *PLoS Genet* **16:** e1009034. doi:10.1371/journal.pgen.1009034

Ernst E, Abramson B, Acosta K, Hoang PTN, Mateo-Elizalde C, Schubert V, Pasaribu B, Hartwick N, Colt K, Aylward A, et al. 2023. The genomes and epigenomes of aquatic plants (Lemnaceae) promote triploid hybridization and clonal reproduction. bioRxiv doi:10.1101/2023.08.02.551673

Fang X, Qi Y. 2016. RNAi in plants: an Argonaute-centered view. *Plant Cell* **28:** 272–285. doi:10.1105/tpc.15.00920

Fang J, Leichter SM, Jiang J, Biswal M, Lu J, Zhang Z-M, Ren W, Zhai J, Cui Q, Zhong X, et al. 2021. Substrate deformation regulates DRM2-mediated DNA methylation in plants. *Sci Adv* **7:** eabd9224. doi:10.1126/sciadv.abd9224

Fang J, Jiang J, Leichter SM, Liu J, Biswal M, Khudaverdyan N, Zhong X, Song J. 2022. Mechanistic basis for maintenance of CHG DNA methylation in plants. *Nat Commun* **13:** 3877. doi:10.1038/s41467-022-31627-3

Fang Y, Tian X, Jin Y, Du A, Ding Y, Liao Z, He K, Zhao Y, Guo L, Xiao Y, et al. 2023. Duckweed evolution: from land back to water. bioRxiv doi:10.1101/2023.03.22.533731

Fei Q, Yang L, Liang W, Zhang D, Meyers BC. 2016. Dynamic changes of small RNAs in rice spikelet development reveal specialized reproductive phasiRNA pathways. *J Exp Bot* **67:** 6037–6049. doi:10.1093/jxb/erw361

Feng S, Zhong Z, Wang M, Jacobsen SE. 2020. Efficient and accurate determination of genome-wide DNA methylation patterns in *Arabidopsis thaliana* with enzymatic methyl sequencing. *Epigenetics Chromatin* **13:** 42. doi:10.1186/s13072-020-00361-9

Feschotte C. 2008. Transposable elements and the evolution of regulatory networks. *Nat Rev Genet* **9:** 397–405. doi:10.1038/nrg2337

Flynn JM, Hubley R, Goubert C, Rosen J, Clark AG, Feschotte C, Smit AF. 2020. RepeatModeler2 for automated genomic discovery of transposable element families. *Proc Natl Acad Sci* **117:** 9451–9457. doi:10.1073/pnas.1921046117

Fourounjian P, Tang J, Tanyolac B, Feng Y, Gelfand B, Kakrana A, Tu M, Wakim C, Meyers BC, Ma J, et al. 2019. Post-transcriptional adaptation of the aquatic plant *Spirodela polyrhiza* under stress and hormonal stimuli. *Plant J* **98:** 1120–1133. doi:10.1111/tpj.14294

Fourounjian P, Slovin J, Messing J. 2021. Flowering and seed production across the Lemnaceae. *Int J Mol Sci* **22:** 2733. doi:10.3390/ijms22052733

Fu S, Gao Z, Birchler J, Han F. 2012. Dicentric chromosome formation and epigenetics of centromere formation in plants. *J Genet Genom* **39:** 125–130. doi:10.1016/j.jgg.2012.01.006

Fuchs J, Demidov D, Houben A, Schubert I. 2006. Chromosomal histone modification patterns: from conservation to diversity. *Trends Plant Sci* **11:** 199–208. doi:10.1016/j.tplants.2006.02.008

Fusaro AF, Matthew L, Smith NA, Curtin SJ, Dedic-Hagan J, Ellacott GA, Watson JM, Wang M, Brosnan C, Carroll BJ, et al. 2006. RNA interference-inducing hairpin RNAs in plants act through the viral defence pathway. *EMBO Rep* **7:** 1168–1175. doi:10.1038/sj.embor.7400837

Gaillochet C, Lohmann JU. 2015. The never-ending story: from pluripotency to plant developmental plasticity. *Development* **142:** 2237–2249. doi:10.1242/dev.117614

Garcia-Ruiz H, Takeda A, Chapman EJ, Sullivan CM, Fahlgren N, Brempelis KJ, Carrington JC. 2010. *Arabidopsis* RNA-dependent RNA polymerases and dicer-like proteins in antiviral defense and small interfering RNA biogenesis during *Turnip mosaic virus* infection. *Plant Cell* **22:** 481–496. doi:10.1105/tpc.109.073056

Goodall GJ, Filipowicz W. 1991. Different effects of intron nucleotide composition and secondary structure on pre-mRNA splicing in monocot and dicot plants. *EMBO J* **10:** 2635–2644. doi:10.1002/j.1460-2075.1991.tb07806.x

Gorinšek B, Gubenšek F, Kordiš D. 2004. Evolutionary genomics of chromoviruses in eukaryotes. *Mol Biol Evol* **21:** 781–798. doi:10.1093/molbev/msh057

Gouil Q, Baulcombe DC. 2016. DNA methylation signatures of the plant chromomethyltransferases. *PLoS Genet* **12:** e1006526. doi:10.1371/journal.pgen.1006526

Grentzinger T, Oberlin S, Schott G, Handler D, Svozil J, Barragan-Borrero V, Humbert A, Duharcourt S, Brennecke J, Voinnet O. 2020. A universal method for the rapid isolation of all known classes of functional silencing small RNAs. *Nucleic Acids Res* **48:** e79. doi:10.1093/nar/gkaa472

Gu Z, Gu L, Eils R, Schlesner M, Brors B. 2014. *circlize* implements and enhances circular visualization in R. *Bioinformatics* **30:** 2811–2812. doi:10.1093/bioinformatics/btu393

Gutzat R, Rembart K, Nussbaumer T, Hofmann F, Pisupati R, Bradamante G, Daubel N, Gaidora A, Lettner N, Donà M, et al. 2020. *Arabidopsis* shoot stem cells display dynamic transcription and DNA methylation patterns. *EMBO J* **39:** e103667. doi:10.15252/embj.2019103667

Haag JR, Brower-Toland B, Krieger EK, Sidorenko L, Nicora CD, Norbeck AD, Irsigler A, LaRue H, Brzeski J, McGinnis K, et al. 2014. Functional diversification of maize RNA polymerase IV and V subtypes via alternative catalytic subunits. *Cell Rep* **9:** 378–390. doi:10.1016/j.celrep.2014.08.067

Hamilton AJ, Voinnet O, Chappell L, Baulcombe DC. 2002. Two classes of short interfering RNA in RNA silencing. *EMBO J* **21:** 4671–4679. doi:10.1093/emboj/cdf464

Harkess A, McLoughlin F, Bilkey N, Elliott K, Emenecker R, Mattoon E, Miller K, Czymmek K, Vierstra RD, Meyers BC, et al. 2021. Improved *Spirodela polyrhiza* genome and proteomic analyses reveal a conserved chromosomal structure with high abundance of chloroplastic proteins favoring energy production. *J Exp Bot* **72:** 2491–2500. doi:10.1093/jxb/erab006

Harkess A, Bewick AJ, Lu Z, Fourounjian P, Michael TP, Schmitz RJ, Meyers BC. 2024. Unusual predominance of maintenance DNA methylation in *Spirodela polyrhiza*. *G3 (Bethesda)* **14:** jkae004. doi:10.1093/g3journal/jkae004

Harvey JJW, Lewsey MG, Patel K, Westwood J, Heimstädt S, Carr JP, Baulcombe DC. 2011. An antiviral defense role of AGO2 in plants. *PLoS One* **6:** e14639. doi:10.1371/journal.pone.0014639

Havecker ER, Wallbridge LM, Hardcastle TJ, Bush MS, Kelly KA, Dunn RM, Schwach F, Doonan JH, Baulcombe DC. 2010. The *Arabidopsis* RNA-directed DNA methylation argonautes functionally diverge based on their expression and interaction with target loci. *Plant Cell* **22:** 321–334. doi:10.1105/tpc.109.072199

Hayashi R, Schnabl J, Handler D, Mohn F, Ameres SL, Brennecke J. 2016. Genetic and mechanistic diversity of piRNA 3′-end formation. *Nature* **539:** 588–592. doi:10.1038/nature20162

He Y, Zhang T, Sun H, Zhan H, Zhao Y. 2020. A reporter for noninvasively monitoring gene expression and plant transformation. *Hortic Res* **7:** 152. doi:10.1038/s41438-020-00390-1

He L, Zhao C, Zhang Q, Zinta G, Wang D, Lozano-Durán R, Zhu J-K. 2021. Pathway conversion enables a double-lock mechanism to maintain DNA methylation and genome stability. *Proc Natl Acad Sci* **118:** e2107320118. doi:10.1073/pnas.2107320118

Henderson IR, Zhang X, Lu C, Johnson L, Meyers BC, Green PJ, Jacobsen SE. 2006. Dissecting *Arabidopsis thaliana* DICER function in small RNA processing, gene silencing and DNA methylation patterning. *Nat Genet* **38:** 721–725. doi:10.1038/ng1804

Henikoff S, Smith MM. 2015. Histone variants and epigenetics. *Cold Spring Harb Perspect Biol* **7:** a019364. doi:10.1101/cshperspect.a019364

Hisanaga T, Romani F, Wu S, Kowar T, Wu Y, Lintermann R, Fridrich A, Cho CH, Chaumier T, Jamge B, et al. 2023. The polycomb repressive complex 2 deposits H3K27me3 and represses transposable elements in a broad

range of eukaryotes. *Curr Biol* **33:** 4367–4380.e9. doi:10.1016/j.cub.2023.08.073

Ho EKH, Bartkowska M, Wright SI, Agrawal AF. 2019. Population genomics of the facultatively asexual duckweed *Spirodela polyrhiza*. *New Phytol* **224:** 1361–1371. doi:10.1111/nph.16056

Hoang PNT, Michael TP, Gilbert S, Chu P, Motley ST, Appenroth KJ, Schubert I, Lam E. 2018. Generating a high-confidence reference genome map of the greater duckweed by integration of cytogenomic, optical mapping, and Oxford Nanopore technologies. *Plant J* **96:** 670–684. doi:10.1111/tpj.14049

Hoang PTN, Fiebig A, Novák P, Macas J, Cao HX, Stepanenko A, Chen G, Borisjuk N, Scholz U, Schubert I. 2020. Chromosome-scale genome assembly for the duckweed *Spirodela intermedia*, integrating cytogenetic maps, PacBio and Oxford Nanopore libraries. *Sci Rep* **10:** 19230. doi:10.1038/s41598-020-75728-9

Houben A, Demidov D, Gernand D, Meister A, Leach CR, Schubert I. 2003. Methylation of histone H3 in euchromatin of plant chromosomes depends on basic nuclear DNA content. *Plant J* **33:** 967–973. doi:10.1046/j.1365-313X.2003.01681.x

Huang Y, Kendall T, Forsythe ES, Dorantes-Acosta A, Li S, Caballero-Pérez J, Chen X, Arteaga-Vázquez M, Beilstein MA, Mosher RA. 2015. Ancient origin and recent innovations of RNA polymerase IV and V. *Mol Biol Evol* **32:** 1788–1799. doi:10.1093/molbev/msv060

Huang X, Zhang S, Li K, Thimmapuram J, Xie S, Wren J. 2018. ViewBS: a powerful toolkit for visualization of high-throughput bisulfite sequencing data. *Bioinformatics* **34:** 708–709. doi:10.1093/bioinformatics/btx633

Huff JT, Zilberman D, Roy SW. 2016. Mechanism for DNA transposons to generate introns on genomic scales. *Nature* **538:** 533–536. doi:10.1038/nature20110

Ibarra-Laclette E, Lyons E, Hernández-Guzmán G, Pérez-Torres CA, Carretero-Paulet L, Chang T-H, Lan T, Welch AJ, Juárez MJA, Simpson J, et al. 2013. Architecture and evolution of a minute plant genome. *Nature* **498:** 94–98. doi:10.1038/nature12132

Ilık İA, Glažar P, Tse K, Brändl B, Meierhofer D, Müller F-J, Smith ZD, Aktaş T. 2024. Autonomous transposons tune their sequences to ensure somatic suppression. *Nature* **626:** 1116–1124. doi:10.1038/s41586-024-07081-0

Incarbone M, Bradamante G, Pruckner F, Wegscheider T, Rozhon W, Nguyen V, Gutzat R, Mérai Z, Lendl T, MacFarlane S, et al. 2023. Salicylic acid and RNA interference mediate antiviral immunity of plant stem cells. *Proc Natl Acad Sci* **120:** e2302069120. doi:10.1073/pnas.2302069120

Ito H, Gaubert H, Bucher E, Mirouze M, Vaillant I, Paszkowski J. 2011. An siRNA pathway prevents transgenerational retrotransposition in plants subjected to stress. *Nature* **472:** 115–119. doi:10.1038/nature09861

Jackson JP, Lindroth AM, Cao X, Jacobsen SE. 2002. Control of CpNpG DNA methylation by the KRYPTONITE histone H3 methyltransferase. *Nature* **416:** 556–560. doi:10.1038/nature731

Jackson JP, Johnson L, Jasencakova Z, Zhang X, PerezBurgos L, Singh PB, Cheng X, Schubert I, Jenuwein T, Jacobsen SE. 2004. Dimethylation of histone H3 lysine 9 is a critical mark for DNA methylation and gene silencing in *Arabidopsis thaliana*. *Chromosoma* **112:** 308–315. doi:10.1007/s00412-004-0275-7

Jacob Y, Feng S, LeBlanc CA, Bernatavichute YV, Stroud H, Cokus S, Johnson LM, Pellegrini M, Jacobsen SE, Michaels SD. 2009. ATXR5 and ATXR6 are H3K27 monomethyltransferases required for chromatin structure and gene silencing. *Nat Struct Mol Biol* **16:** 763–768. doi:10.1038/nsmb.1611

Jamge B, Lorković ZJ, Axelsson E, Osakabe A, Shukla V, Yelagandula R, Akimcheva S, Kuehn AL, Berger F. 2023. Histone variants shape chromatin states in *Arabidopsis*. *eLife* **12:** RP87714. doi:10.7554/eLife.87714

Jasencakova Z, Soppe WJJ, Meister A, Gernand D, Turner BM, Schubert I. 2003. Histone modifications in *Arabidopsis*: high methylation of H3 lysine 9 is dispensable for constitutive heterochromatin. *Plant J* **33:** 471–480. doi:10.1046/j.1365-313X.2003.01638.x

Jay F, Brioudes F, Voinnet O. 2023. A contemporary reassessment of the enhanced transient expression system based on the tombusviral silencing suppressor protein P19. *Plant J* **113:** 186–204. doi:10.1111/tpj.16032

Jia J, Ji R, Li Z, Yu Y, Nakano M, Long Y, Feng L, Qin C, Lu D, Zhan J, et al. 2020. Soybean DICER-LIKE2 regulates seed coat color via production of primary 22-nucleotide small interfering RNAs from long inverted repeats. *Plant Cell* **32:** 3662–3673. doi:10.1105/tpc.20.00562

Johnson L, Mollah S, Garcia BA, Muratore TL, Shabanowitz J, Hunt DF, Jacobsen SE. 2004. Mass spectrometry analysis of *Arabidopsis* histone H3 reveals distinct combinations of post-translational modifications. *Nucleic Acids Res* **32:** 6511–6518. doi:10.1093/nar/gkh992

Johnson LM, Bostick M, Zhang X, Kraft E, Henderson I, Callis J, Jacobsen SE. 2007. The SRA methyl-cytosine-binding domain links DNA and histone methylation. *Curr Biol* **17:** 379–384. doi:10.1016/j.cub.2007.01.009

Johnson LM, Law JA, Khattar A, Henderson IR, Jacobsen SE. 2008. SRA-domain proteins required for DRM2-mediated de novo DNA methylation. *PLoS Genet* **4:** e1000280. doi:10.1371/journal.pgen.1000280

Johnson LM, Du J, Hale CJ, Bischof S, Feng S, Chodavarapu RK, Zhong X, Marson G, Pellegrini M, Segal DJ, et al. 2014. SRA- and SET-domain-containing proteins link RNA polymerase V occupancy to DNA methylation. *Nature* **507:** 124–128. doi:10.1038/nature12931

Jullien PE, Grob S, Marchais A, Pumplin N, Chevalier C, Bonnet DMV, Otto C, Schott G, Voinnet O. 2020. Functional characterization of *Arabidopsis* ARGONAUTE 3 in reproductive tissues. *Plant J* **103:** 1796–1809. doi:10.1111/tpj.14868

Keith B, Chua N-H. 1986. Monocot and dicot pre-mRNAs are processed with different efficiencies in transgenic tobacco. *EMBO J* **5:** 2419–2425. doi:10.1002/j.1460-2075.1986.tb04516.x

Kim MY, Zilberman D. 2014. DNA methylation as a system of plant genomic immunity. *Trends Plant Sci* **19:** 320–326. doi:10.1016/j.tplants.2014.01.014

Klein SP, Anderson SN. 2022. The evolution and function of transposons in epigenetic regulation in response to the environment. *Curr Opin Plant Biol* **69:** 102277. doi:10.1016/j.pbi.2022.102277

Krueger F, Andrews SR. 2011. Bismark: a flexible aligner and methylation caller for bisulfite-seq applications. *Bioinformatics* **27:** 1571–1572. doi:10.1093/bioinformatics/btr167

Krzywinski M, Schein J, Birol I, Connors J, Gascoyne R, Horsman D, Jones SJ, Marra MA. 2009. Circos: an information aesthetic for comparative genomics. *Genome Res* **19:** 1639–1645. doi:10.1101/gr.092759.109

Kumar A, Bennetzen JL. 1999. Plant retrotransposons. *Annu Rev Genet* **33:** 479–532. doi:10.1146/annurev.genet.33.1.479

Lam E, Michael TP. 2022. Wolffia, a minimalist plant and synthetic biology chassis. *Trends Plant Sci* **27:** 430–439. doi:10.1016/j.tplants.2021.11.014

Landolt E. 1986. *Biosystematic investigations in the family of duckweeds (Lemnaceae) (Vol 2). The family of lemnaceae—a monographic study*. Veroeffentlichungen des Geobotanischen Instituts der ETH, Stiftung Ruebel, Switzerland.

Langmead B, Salzberg SL. 2012. Fast gapped-read alignment with Bowtie 2. *Nat Methods* **9:** 357–359. doi:10.1038/nmeth.1923

Law JA, Vashisht AA, Wohlschlegel JA, Jacobsen SE. 2011. SHH1, a homeodomain protein required for DNA methylation, as well as RDR2, RDM4, and chromatin remodeling factors, associate with RNA polymerase IV. *PLoS Genet* **7:** e1002195. doi:10.1371/journal.pgen.1002195

Law JA, Du J, Hale CJ, Feng S, Krajewski K, Palanca AMS, Strahl BD, Patel DJ, Jacobsen SE. 2013. Polymerase IV occupancy at RNA-directed DNA methylation sites requires SHH1. *Nature* **498:** 385–389. doi:10.1038/nature12178

Lee SC, Ernst E, Berube B, Borges F, Parent J-S, Ledon P, Schorn A, Martienssen RA. 2020. *Arabidopsis* retrotransposon virus-like particles and their regulation by epigenetically activated small RNA. *Genome Res* **30:** 576–588. doi:10.1101/gr.259044.119

Lee Y-S, Maple R, Dürr J, Dawson A, Tamim S, del Genio C, Papareddy R, Luo A, Lamb JC, Amantia S, et al. 2021. A transposon surveillance mechanism that safeguards plant male fertility during stress. *Nat Plants* **7:** 34–41. doi:10.1038/s41477-020-00818-5

Lemon GD, Posluszny U. 2000. Comparative shoot development and evolution in the Lemnaceae. *Int J Plant Sci* **161:** 733–748. doi:10.1086/314298

Li H. 2021. New strategies to improve minimap2 alignment accuracy. *Bioinformatics* **37:** 4572–4574. doi:10.1093/bioinformatics/btab705

Li H, Handsaker B, Wysoker A, Fennell T, Ruan J, Homer N, Marth G, Abecasis G, Durbin R, 1000 Genome Project Data Processing Subgroup. 2009. The Sequence Alignment/Map format and SAMtools. *Bioinformatics* **25:** 2078–2079. doi:10.1093/bioinformatics/btp352

Li X, Harris CJ, Zhong Z, Chen W, Liu R, Jia B, Wang Z, Li S, Jacobsen SE, Du J. 2018. Mechanistic insights into plant SUVH family H3K9 methyltransferases and their binding to context-biased non-CG DNA methylation. *Proc Natl Acad Sci* **115:** E8793–E8802. doi:10.1073/pnas.1809841115

Li F, Yang J-J, Sun Z-Y, Wang L, Qi L-Y, A S, Liu Y-Q, Zhang H-M, Dang L-F, Wang S-J, et al. 2023a. Plant-on-chip: core morphogenesis processes in the tiny plant *Wolffia australiana*. *PNAS Nexus* **2:** pgad141. doi:10.1093/pnasnexus/pgad141

Li Z, Wang M, Zhong Z, Gallego-Bartolomé J, Feng S, Jami-Alahmadi Y, Wang X, Wohlschlegel J, Bischof S, Long JA, et al. 2023b. The MOM1 complex recruits the RdDM machinery via MORC6 to establish de novo DNA methylation. *Nat Commun* **14:** 4135. doi:10.1038/s41467-023-39751-4

Liu J, He Z. 2020. Small DNA methylation, big player in plant abiotic stress responses and memory. *Front Plant Sci* **11:** 595603. doi:10.3389/fpls.2020.595603

Liu Z-W, Shao C-R, Zhang C-J, Zhou J-X, Zhang S-W, Li L, Chen S, Huang H-W, Cai T, He X-J. 2014. The SET domain proteins SUVH2 and SUVH9 are

required for Pol V occupancy at RNA-directed DNA methylation loci. *PLoS Genet* **10:** e1003948. doi:10.1371/journal.pgen.1003948
Liu W, Duttke SH, Hetzel J, Groth M, Feng S, Gallego-Bartolome J, Zhong Z, Kuo HY, Wang Z, Zhai J, et al. 2018. RNA-directed DNA methylation involves co-transcriptional small-RNA-guided slicing of polymerase V transcripts in *Arabidopsis*. *Nat Plants* **4:** 181–188. doi:10.1038/s41477-017-0100-y
Liu Y, Teng C, Xia R, Meyers BC. 2020. PhasiRNAs in plants: their biogenesis, genic sources, and roles in stress responses, development, and reproduction. *Plant Cell* **32:** 3059–3080. doi:10.1105/tpc.20.00335
Llave C, Kasschau KD, Rector MA, Carrington JC. 2002. Endogenous and silencing-associated small RNAs in plants. *Plant Cell* **14:** 1605–1619. doi:10.1105/tpc.003210
Loffer A, Singh J, Fukudome A, Mishra V, Wang F, Pikaard CS. 2022. A DCL3 dicing code within Pol IV-RDR2 transcripts diversifies the siRNA pool guiding RNA-directed DNA methylation. *eLife* **11:** e73260. doi:10.7554/eLife.73260
Long J, Walker J, She W, Aldridge B, Gao H, Deans S, Vickers M, Feng X. 2021. Nurse cell–derived small RNAs define paternal epigenetic inheritance in *Arabidopsis*. *Science* **373:** eabh0556. doi:10.1126/science.abh0556
Lou H, McCullough AJ, Schuler MA. 1993. Expression of maize *Adh1* intron mutants in tobacco nuclei. *Plant J* **3:** 393–403. doi:10.1046/j.1365-313X.1993.t01-22-00999.x
Malone CD, Hannon GJ. 2009. Small RNAs as guardians of the genome. *Cell* **136:** 656–668. doi:10.1016/j.cell.2009.01.045
Marí-Ordóñez A, Marchais A, Etcheverry M, Martin A, Colot V, Voinnet O. 2013. Reconstructing de novo silencing of an active plant retrotransposon. *Nat Genet* **45:** 1029–1039. doi:10.1038/ng.2703
Mathieu O, Probst AV, Paszkowski J. 2005. Distinct regulation of histone H3 methylation at lysines 27 and 9 by CpG methylation in *Arabidopsis*. *EMBO J* **24:** 2783–2791. doi:10.1038/sj.emboj.7600743
Mathieu O, Reinders J, Čaikovski M, Smathajitt C, Paszkowski J. 2007. Transgenerational stability of the *Arabidopsis* epigenome is coordinated by CG methylation. *Cell* **130:** 851–862. doi:10.1016/j.cell.2007.07.007
McCue AD, Panda K, Nuthikattu S, Choudury SG, Thomas EN, Slotkin RK. 2015. ARGONAUTE 6 bridges transposable element mRNA-derived siRNAs to the establishment of DNA methylation. *EMBO J* **34:** 20–35. doi:10.15252/embj.201489499
McKenna A, Hanna M, Banks E, Sivachenko A, Cibulskis K, Kernytsky A, Garimella K, Altshuler D, Gabriel S, Daly M, et al. 2010. The Genome Analysis Toolkit: a MapReduce framework for analyzing next-generation DNA sequencing data. *Genome Res* **20:** 1297–1303. doi:10.1101/gr.107524.110
Mi S, Cai T, Hu Y, Chen Y, Hodges E, Ni F, Wu L, Li S, Zhou H, Long C, et al. 2008. Sorting of small RNAs into *Arabidopsis* argonaute complexes is directed by the 5′ terminal nucleotide. *Cell* **133:** 116–127. doi:10.1016/j.cell.2008.02.034
Michael TP, Bryant D, Gutierrez R, Borisjuk N, Chu P, Zhang H, Xia J, Zhou J, Peng H, Baidouri ME, et al. 2017. Comprehensive definition of genome features in *Spirodela polyrhiza* by high-depth physical mapping and short-read DNA sequencing strategies. *Plant J* **89:** 617–635. doi:10.1111/tpj.13400
Michael TP, Ernst E, Hartwick N, Chu P, Bryant D, Gilbert S, Ortleb S, Baggs EL, Sree KS, Appenroth KJ, et al. 2021. Genome and time-of-day transcriptome of *Wolffia australiana* link morphological minimization with gene loss and less growth control. *Genome Res* **31:** 225–238. doi:10.1101/gr.266429.120
Mirouze M, Reinders J, Bucher E, Nishimura T, Schneeberger K, Ossowski S, Cao J, Weigel D, Paszkowski J, Mathieu O. 2009. Selective epigenetic control of retrotransposition in *Arabidopsis*. *Nature* **461:** 427–430. doi:10.1038/nature08328
Moazed D. 2009. Small RNAs in transcriptional gene silencing and genome defence. *Nature* **457:** 413–420. doi:10.1038/nature07756
Montavon T, Kwon Y, Zimmermann A, Hammann P, Vincent T, Cognat V, Michel F, Dunoyer P. 2017. A specific dsRNA-binding protein complex selectively sequesters endogenous inverted-repeat siRNA precursors and inhibits their processing. *Nucleic Acids Res* **45:** 1330–1344. doi:10.1093/nar/gkw1264
Montgomery SA, Tanizawa Y, Galik B, Wang N, Ito T, Mochizuki T, Akimcheva S, Bowman JL, Cognat V, Maréchal-Drouard L, et al. 2020. Chromatin organization in early land plants reveals an ancestral association between H3K27me3, transposons, and constitutive heterochromatin. *Curr Biol* **30:** 573–588.e7. doi:10.1016/j.cub.2019.12.015
Morello L, Braglia L, Iannelli MA, Lauria M, Gavazzi F, Gianì S, Perna C. 2024. IBBA Duckweed Dataset (DUCKWEED-01). Institute of Agricultural Biology and Biotechnology (IBBA), National Research Council of Italy (CNR), Milano, Italy. Occurrence dataset. https://doi.org/10.15468/hstsnr
Neumann P, Novák P, Hoštáková N, Macas J. 2019. Systematic survey of plant LTR-retrotransposons elucidates phylogenetic relationships of their polyprotein domains and provides a reference for element classification. *Mob DNA* **10:** 1. doi:10.1186/s13100-018-0144-1
Nguyen V, Gutzat R. 2022. Epigenetic regulation in the shoot apical meristem. *Curr Opin Plant Biol* **69:** 102267. doi:10.1016/j.pbi.2022.102267
Niederhuth CE, Bewick AJ, Ji L, Alabady MS, Kim KD, Li Q, Rohr NA, Rambani A, Burke JM, Udall JA, et al. 2016. Widespread natural variation of DNA methylation within angiosperms. *Genome Biol* **17:** 194. doi:10.1186/s13059-016-1059-0
Nielsen CPS, Han L, Arribas-Hernández L, Karelina D, Petersen M, Brodersen P. 2023. Sensing of viral RNA in plants via a DICER-LIKE ribonuclease. bioRxiv doi:10.1101/2023.01.10.523395
Nielsen CPS, Arribas-Hernández L, Han L, Reichel M, Woessmann J, Daucke R, Bressendorff S, López-Márquez D, Andersen SU, Pumplin N, et al. 2024. Evidence for an RNAi-independent role of *Arabidopsis* DICER-LIKE2 in growth inhibition and basal antiviral resistance. *Plant Cell* **36:** 2289–2309. doi:10.1093/plcell/koae067
Nuthikattu S, McCue AD, Panda K, Fultz D, DeFraia C, Thomas EN, Slotkin RK. 2013. The initiation of epigenetic silencing of active transposable elements is triggered by RDR6 and 21-22 nucleotide small interfering RNAs. *Plant Physiol* **162:** 116–131. doi:10.1104/pp.113.216481
Oberlin S, Sarazin A, Chevalier C, Voinnet O, Marí-Ordóñez A. 2017. A genome-wide transcriptome and translatome analysis of *Arabidopsis* transposons identifies a unique and conserved genome expression strategy for *Ty1/Copia* retroelements. *Genome Res* **27:** 1549–1562. doi:10.1101/gr.220723.117
Oberlin S, Rajeswaran R, Trasser M, Barragán-Borrero V, Schon MA, Plotnikova A, Loncsek L, Nodine MD, Marí-Ordóñez A, Voinnet O. 2022. Innate, translation-dependent silencing of an invasive transposon in *Arabidopsis*. *EMBO Rep* **23:** e53400. doi:10.15252/embr.202153400
Osakabe A, Jamge B, Axelsson E, Montgomery SA, Akimcheva S, Kuehn AL, Pisupati R, Lorković ZJ, Yelagandula R, Kakutani T, et al. 2021. The chromatin remodeler DDM1 prevents transposon mobility through deposition of histone variant H2A.W. *Nat Cell Biol* **23:** 391–400. doi:10.1038/s41556-021-00658-1
Ou S, Su W, Liao Y, Chougule K, Agda JRA, Hellinga AJ, Lugo CSB, Elliott TA, Ware D, Peterson T, et al. 2019. Benchmarking transposable element annotation methods for creation of a streamlined, comprehensive pipeline. *Genome Biol* **20:** 275. doi:10.1186/s13059-019-1905-y
Panda K, McCue AD, Slotkin RK. 2020. *Arabidopsis* RNA polymerase IV generates 21–22 nucleotide small RNAs that can participate in RNA-directed DNA methylation and may regulate genes. *Philos Trans R Soc Lond B Biol Sci* **375:** 20190417. doi:10.1098/rstb.2019.0417
Parent J, Bouteiller N, Elmayan T, Vaucheret H. 2015. Respective contributions of *Arabidopsis* DCL2 and DCL4 to RNA silencing. *Plant J* **81:** 223–232. doi:10.1111/tpj.12720
Parhad SS, Theurkauf WE. 2019. Rapid evolution and conserved function of the piRNA pathway. *Open Biol* **9:** 180181. doi:10.1098/rsob.180181
Patel P, Mathioni SM, Hammond R, Harkess AE, Kakrana A, Arikit S, Dusia A, Meyers BC. 2021. Reproductive phasiRNA loci and DICER-LIKE5, but not microRNA loci, diversified in monocotyledonous plants. *Plant Physiol* **185:** 1764–1782. doi:10.1093/plphys/kiab001
Pieterse AH. 2013. Is flowering in Lemnaceae stress-induced? A review. *Aquat Bot* **104:** 1–4. doi:10.1016/j.aquabot.2012.08.002
Poplin R, Ruano-Rubio V, DePristo MA, Fennell TJ, Carneiro MO, der Auwera GAV, Kling DE, Gauthier LD, Levy-Moonshine A, Roazen D, et al. 2018. Scaling accurate genetic variant discovery to tens of thousands of samples. bioRxiv doi:10.1101/201178
Pratx L, Wendering P, Kappel C, Nikoloski Z, Bäurle I. 2023. Histone retention preserves epigenetic marks during heat stress-induced transcriptional memory in plants. *EMBO J* **42:** e113595. doi:10.15252/embj.2023113595
Quinlan AR, Hall IM. 2010. BEDTools: a flexible suite of utilities for comparing genomic features. *Bioinformatics* **26:** 841–842. doi:10.1093/bioinformatics/btq033
Rajakumara E, Law JA, Simanshu DK, Voigt P, Johnson LM, Reinberg D, Patel DJ, Jacobsen SE. 2011. A dual flip-out mechanism for 5mC recognition by the *Arabidopsis* SUVH5 SRA domain and its impact on DNA methylation and H3K9 dimethylation in vivo. *Genes Dev* **25:** 137–152. doi:10.1101/gad.1980311
Ramírez F, Ryan DP, Grüning B, Bhardwaj V, Kilpert F, Richter AS, Heyne S, Dündar F, Manke T. 2016. deepTools2: a next generation web server for deep-sequencing data analysis. *Nucleic Acids Res* **44:** W160–W165. doi:10.1093/nar/gkw257
Regulski M, Lu Z, Kendall J, Donoghue MTA, Reinders J, Llaca V, Deschamps S, Smith A, Levy D, McCombie WR, et al. 2013. The maize methylome influences mRNA splice sites and reveals widespread paramutation-like switches guided by small RNA. *Genome Res* **23:** 1651–1662. doi:10.1101/gr.153510.112
Reinders J, Wulff BBH, Mirouze M, Ordóñez AM, Dapp M, Rozhon W, Bucher E, Theiler G, Paszkowski J. 2009. Compromised stability of

DNA methylation and transposon immobilization in mosaic *Arabidopsis* epigenomes. *Genes Dev* **23:** 939–950. doi:10.1101/gad.524609

Roudier F, Ahmed I, Bérard C, Sarazin A, Mary-Huard T, Cortijo S, Bouyer D, Caillieux E, Duvernois-Berthet E, Al-Shikhley L, et al. 2011. Integrative epigenomic mapping defines four main chromatin states in *Arabidopsis*. *EMBO J* **30:** 1928–1938. doi:10.1038/emboj.2011.103

Rougée M, Quadrana L, Zervudacki J, Hure V, Colot V, Navarro L, Deleris A. 2021. Polycomb mutant partially suppresses DNA hypomethylation–associated phenotypes in *Arabidopsis*. *Life Sci Alliance* **4:** e202000848. doi:10.26508/lsa.202000848

Rowley MJ, Avrutsky MI, Sifuentes CJ, Pereira L, Wierzbicki AT. 2011. Independent chromatin binding of ARGONAUTE4 and SPT5L/KTF1 mediates transcriptional gene silencing. *PLoS Genet* **7:** e1002120. doi:10.1371/journal.pgen.1002120

Sammarco I, Pieters J, Salony S, Toman I, Zolotarov G, Placette CL. 2022. Epigenetic targeting of transposon relics: beating the dead horses of the genome? *Epigenetics* **17:** 1331–1344. doi:10.1080/15592294.2021.2022066

Saze H, Kitayama J, Takashima K, Miura S, Harukawa Y, Ito T, Kakutani T. 2013. Mechanism for full-length RNA processing of *Arabidopsis* genes containing intragenic heterochromatin. *Nat Commun* **4:** 2301. doi:10.1038/ncomms3301

Scheid R, Dowell JA, Sanders D, Jiang J, Denu JM, Zhong X. 2022. Histone acid extraction and high throughput mass spectrometry to profile histone modifications in *Arabidopsis thaliana*. *Curr Protoc* **2:** e527. doi:10.1002/cpz1.527

Schultz MD, He Y, Whitaker JW, Hariharan M, Mukamel EA, Leung D, Rajagopal N, Nery JR, Urich MA, Chen H, et al. 2015. Human body epigenome maps reveal noncanonical DNA methylation variation. *Nature* **523:** 212–216. doi:10.1038/nature14465

Sequeira-Mendes J, Aragüez I, Peiró R, Mendez-Giraldez R, Zhang X, Jacobsen SE, Bastolla U, Gutierrez C. 2014. The functional topography of the *Arabidopsis* genome is organized in a reduced number of linear motifs of chromatin states. *Plant Cell* **26:** 2351–2366. doi:10.1105/tpc.114.124578

Seymour DK, Koenig D, Hagmann J, Becker C, Weigel D. 2014. Evolution of DNA methylation patterns in the Brassicaceae is driven by differences in genome organization. *PLoS Genet* **10:** e1004785. doi:10.1371/journal.pgen.1004785

Shamandi N, Zytnicki M, Charbonnel C, Elvira-Matelot E, Bochnakian A, Comella P, Mallory AC, Lepère G, Sáez-Vásquez J, Vaucheret H. 2015. Plants encode a general siRNA suppressor that is induced and suppressed by viruses. *PLoS Biol* **13:** e1002326. doi:10.1371/journal.pbio.1002326

Shi J, Dawe RK. 2006. Partitioning of the maize epigenome by the number of methyl groups on histone H3 lysines 9 and 27. *Genetics* **173:** 1571–1583. doi:10.1534/genetics.106.056853

Shumate A, Salzberg SL. 2021. Liftoff: accurate mapping of gene annotations. *Bioinformatics* **37:** 1639–1643. doi:10.1093/bioinformatics/btaa1016

Sigman MJ, Slotkin RK. 2016. The first rule of plant transposable element silencing: location, location, location. *Plant Cell* **28:** 304–313. doi:10.1105/tpc.15.00869

Sigman MJ, Panda K, Kirchner R, McLain LL, Payne H, Peasari JR, Husbands AY, Slotkin RK, McCue AD. 2021. An siRNA-guided ARGONAUTE protein directs RNA polymerase V to initiate DNA methylation. *Nat Plants* **7:** 1461–1474. doi:10.1038/s41477-021-01008-7

Simon L, Rabanal FA, Dubos T, Oliver C, Lauber D, Poulet A, Vogt A, Mandlbauer A, Le Goff S, Sommer A, et al. 2018. Genetic and epigenetic variation in 5S ribosomal RNA genes reveals genome dynamics in *Arabidopsis thaliana*. *Nucleic Acids Res* **46:** 3019–3033. doi:10.1093/nar/gky163

Slotkin RK, Vaughn M, Borges F, Tanurdžić M, Becker JD, Feijó JA, Martienssen RA. 2009. Epigenetic reprogramming and small RNA silencing of transposable elements in pollen. *Cell* **136:** 461–472. doi:10.1016/j.cell.2008.12.038

Sree KS, Maheshwari SC, Boka K, Khurana JP, Keresztes Á, Appenroth K-J. 2015. The duckweed *Wolffia microscopica*: a unique aquatic monocot. *Flora Morphol Distrib Funct Ecol Plants* **210:** 31–39. doi:10.1016/j.flora.2014.10.006

Stroud H, Hale CJ, Feng S, Caro E, Jacob Y, Michaels SD, Jacobsen SE. 2012. DNA methyltransferases are required to induce heterochromatic re-replication in *Arabidopsis*. *PLoS Genet* **8:** e1002808. doi:10.1371/journal.pgen.1002808

Stroud H, Greenberg MVC, Feng S, Bernatavichute YV, Jacobsen SE. 2013. Comprehensive analysis of silencing mutants reveals complex regulation of the *Arabidopsis* methylome. *Cell* **152:** 352–364. doi:10.1016/j.cell.2012.10.054

Stroud H, Do T, Du J, Zhong X, Feng S, Johnson L, Patel DJ, Jacobsen SE. 2014. Non-CG methylation patterns shape the epigenetic landscape in *Arabidopsis*. *Nat Struct Mol Biol* **21:** 64–72. doi:10.1038/nsmb.2735

Sun S, Kang X-P, Xing X-J, Chen Z-F, Zheng S-W, Xing G-M. 2014. Transient expression of siRNA targeted against the TYLCV AV1, AC1 and AC3 genes for high resistance in tomato. *Sci Hortic* **179:** 321–327. doi:10.1016/j.scienta.2014.10.002

Šurbanovski N, Brilli M, Moser M, Si-Ammour A. 2016. A highly specific microRNA-mediated mechanism silences LTR retrotransposons of strawberry. *Plant J* **85:** 70–82. doi:10.1111/tpj.13090

Taochy C, Gursanscky NR, Cao J, Fletcher SJ, Dressel U, Mitter N, Tucker MR, Koltunow AMG, Bowman JL, Vaucheret H, et al. 2017. A genetic screen for impaired systemic RNAi highlights the crucial role of DICER-LIKE 2. *Plant Physiol* **175:** 1424–1437. doi:10.1104/pp.17.01181

Teixeira FK, Heredia F, Sarazin A, Roudier F, Boccara M, Ciaudo C, Cruaud C, Poulain J, Berdasco M, Fraga MF, et al. 2009. A role for RNAi in the selective correction of DNA methylation defects. *Science* **323:** 1600–1604. doi:10.1126/science.1165313

Tippery NP, Les DH, Appenroth KJ, Sree KS, Crawford DJ, Bog M. 2021. Lemnaceae and Orontiaceae are phylogenetically and morphologically distinct from Araceae. *Plants* **10:** 2639. doi:10.3390/plants10122639

Tirot L, Jullien PE, Ingouff M. 2021. Evolution of CG methylation maintenance machinery in plants. *Epigenomes* **5:** 19. doi:10.3390/epigenomes5030019

Trujillo JT, Beilstein MA, Mosher RA. 2016. The Argonaute-binding platform of NRPE1 evolves through modulation of intrinsically disordered repeats. *New Phytol* **212:** 1094–1105. doi:10.1111/nph.14089

Tschopp M-A, Iki T, Brosnan CA, Jullien PE, Pumplin N. 2017. A complex of *Arabidopsis* DRB proteins can impair dsRNA processing. *RNA* **23:** 782–797. doi:10.1261/rna.059519.116

Tsukahara S, Kobayashi A, Kawabe A, Mathieu O, Miura A, Kakutani T. 2010. Bursts of retrotransposition reproduced in *Arabidopsis*. *Nature* **461:** 423–426. doi:10.1038/nature08351

Urquiaga MCDO, Thiebaut F, Hemerly AS, Ferreira PCG. 2021. From trash to luxury: the potential role of plant LncRNA in DNA methylation during abiotic stress. *Front Plant Sci* **11:** 603246. doi:10.3389/fpls.2020.603246

Walter M, Teissandier A, Pérez-Palacios R, Bourc'his D. 2016. An epigenetic switch ensures transposon repression upon dynamic loss of DNA methylation in embryonic stem cells. *eLife* **5:** e11418. doi:10.7554/eLife.11418

Wang Z, Baulcombe DC. 2020. Transposon age and non-CG methylation. *Nat Commun* **11:** 1221. doi:10.1038/s41467-020-14995-6

Wang X, Duan C-G, Tang K, Wang B, Zhang H, Lei M, Lu K, Mangrauthia SK, Wang P, Zhu G, et al. 2013. RNA-binding protein regulates plant DNA methylation by controlling mRNA processing at the intronic heterochromatin-containing gene *IBM1*. *Proc Natl Acad Sci* **110:** 15467–15472. doi:10.1073/pnas.1315399110

Wang W, Haberer G, Gundlach H, Gläßer C, Nussbaumer T, Luo MC, Lomsadze A, Borodovsky M, Kerstetter RA, Shanklin J, et al. 2014. The *Apirodela polyrhiza* genome reveals insights into its neotenous reduction fast growth and aquatic lifestyle. *Nat Commun* **5:** 3311. doi:10.1038/ncomms4311

Wang T, Deng Z, Zhang X, Wang H, Wang Y, Liu X, Liu S, Xu F, Li T, Fu D, et al. 2018. Tomato *DCL2b* is required for the biosynthesis of 22-nt small RNAs, the resulting secondary siRNAs, and the host defense against ToMV. *Hortic Res* **5:** 62. doi:10.1038/s41438-018-0073-7

Wang Y, Zhou X, Luo J, Lv S, Liu R, Du X, Jia B, Yuan F, Zhang H, Du J. 2021. Recognition of H3K9me1 by maize RNA-directed DNA methylation factor SHH2. *J Integr Plant Biol* **63:** 1091–1096. doi:10.1111/jipb.13103

Wang Y, Duchen P, Chávez A, Sree KS, Appenroth KJ, Zhao H, Höfer M, Huber M, Xu S. 2024. Population genomics and epigenomics of *Apirodela polyrhiza* provide insights into the evolution of facultative asexuality. *Commun Biol* **7:** 581. doi:10.1038/s42003-024-06266-7

Ware A, Jones DH, Flis P, Chrysanthou E, Smith KE, Kümpers BMC, Yant L, Atkinson JA, Wells DM, Bhosale R, et al. 2023. Loss of ancestral function in duckweed roots is accompanied by progressive anatomical reduction and a re-distribution of nutrient transporters. *Curr Biol* **33:** 1795–1802.e4. doi:10.1016/j.cub.2023.03.025

Wells JN, Feschotte C. 2020. A field guide to eukaryotic transposable elements. *Annu Rev Genet* **54:** 539–561. doi:10.1146/annurev-genet-040620-022145

Wendte JM, Zhang Y, Ji L, Shi X, Hazarika RR, Shahryary Y, Johannes F, Schmitz RJ. 2019. Epimutations are associated with CHROMOMETHYLASE 3-induced de novo DNA methylation. *eLife* **8:** e47891. doi:10.7554/eLife.47891

Wicker T, Sabot F, Hua-Van A, Bennetzen JL, Capy P, Chalhoub B, Flavell A, Leroy P, Morgante M, Panaud O, et al. 2007. A unified classification system for eukaryotic transposable elements. *Nat Rev Genet* **8:** 973–982. doi:10.1038/nrg2165

Wickham H. 2009. *ggplot2: elegant graphics for data analysis*. Springer, New York.

Wierzbicki AT, Ream TS, Haag JR, Pikaard CS. 2009. RNA polymerase V transcription guides ARGONAUTE4 to chromatin. *Nat Genet* **41:** 630–634. doi:10.1038/ng.365

Willmann MR, Endres MW, Cook RT, Gregory BD. 2011. The functions of RNA-dependent RNA polymerases in *Arabidopsis*. *Arab Book* **9:** e0146. doi:10.1199/tab.0146

Wright S, Finnegan D. 2001. Genome evolution: sex and the transposable element. *Curr Biol* **11:** R296–R299. doi:10.1016/S0960-9822(01)00168-3

Wyler M, Stritt C, Walser J-C, Baroux C, Roulin AC. 2020. Impact of transposable elements on methylation and gene expression across natural accessions of *Brachypodium distachyon*. *Genome Biol Evol* **12:** 1994–2001. doi:10.1093/gbe/evaa180

Xie Z, Johansen LK, Gustafson AM, Kasschau KD, Lellis AD, Zilberman D, Jacobsen SE, Carrington JC. 2004. Genetic and functional diversification of small RNA pathways in plants. *PLoS Biol* **2:** E104. doi:10.1371/journal.pbio.0020104

Xie Z, Allen E, Wilken A, Carrington JC. 2005. DICER-LIKE 4 functions in *trans*-acting small interfering RNA biogenesis and vegetative phase change in *Arabidopsis thaliana*. *Proc Natl Acad Sci* **102:** 12984–12989. doi:10.1073/pnas.0506426102

Xu S, Stapley J, Gablenz S, Boyer J, Appenroth KJ, Sree KS, Gershenzon J, Widmer A, Huber M. 2019. Low genetic variation is associated with low mutation rate in the giant duckweed. *Nat Commun* **10:** 1243. doi:10.1038/s41467-019-09235-5

Yaari R, Noy-Malka C, Wiedemann G, Gershovitz NA, Reski R, Katz A, Ohad N. 2015. DNA METHYLTRANSFERASE 1 is involved in mCG and mCCG DNA methylation and is essential for sporophyte development in *Physcomitrella patens*. *Plant Mol Biol* **88:** 387–400. doi:10.1007/s11103-015-0328-8

Yan H, Bombarely A, Li S. 2020. DeepTE: a computational method for de novo classification of transposons with convolutional neural network. *Bioinformatics* **36:** 4269–4275. doi:10.1093/bioinformatics/btaa519

Yang G-L, Fang Y, Xu Y-L, Tan L, Li Q, Liu Y, Lai F, Jin Y-L, Du A-P, He K-Z, et al. 2018. Frond transformation system mediated by *Agrobacterium tumefaciens* for *Lemna minor*. *Plant Mol Biol* **98:** 319–331. doi:10.1007/s11103-018-0778-x

Yang J, Zhao X, Li G, Hu S, Hou H. 2021. Frond architecture of the rootless duckweed *Wolffia globosa*. *BMC Plant Biol* **21:** 387. doi:10.1186/s12870-021-03165-5

Yoshikawa M, Peragine A, Park MY, Poethig RS. 2005. A pathway for the biogenesis of *trans*-acting siRNAs in *Arabidopsis*. *Genes Dev* **19:** 2164–2175. doi:10.1101/gad.1352605

Yu D, Fan B, MacFarlane SA, Chen Z. 2003. Analysis of the involvement of an inducible *Arabidopsis* RNA-dependent RNA polymerase in antiviral defense. *Mol Plant Microbe Interact* **16:** 206–216. doi:10.1094/MPMI.2003.16.3.206

Zattera ML, Bruschi DP. 2022. Transposable elements as a source of novel repetitive DNA in the eukaryote genome. *Cells* **11:** 3373. doi:10.3390/cells11213373

Zemach A, Kim MY, Hsieh P-H, Coleman-Derr D, Eshed-Williams L, Thao K, Harmer SL, Zilberman D. 2013. The *Arabidopsis* nucleosome remodeler DDM1 allows DNA methyltransferases to access H1-containing heterochromatin. *Cell* **153:** 193–205. doi:10.1016/j.cell.2013.02.033

Zervudacki J, Yu A, Amesefe D, Wang J, Drouaud J, Navarro L, Deleris A. 2018. Transcriptional control and exploitation of an immune-responsive family of plant retrotransposons. *EMBO J* **37:** e98482. doi:10.15252/embj.201798482

Zhai J, Zhang H, Arikit S, Huang K, Nan G-L, Walbot V, Meyers BC. 2015. Spatiotemporally dynamic, cell-type–dependent premeiotic and meiotic phasiRNAs in maize anthers. *Proc Natl Acad Sci* **112:** 3146–3151. doi:10.1073/pnas.1418918112

Zhan J, Meyers BC. 2023. Plant small RNAs: their biogenesis, regulatory roles, and functions. *Annu Rev Plant Biol* **74:** 21–51. doi:10.1146/annurev-arplant-070122-035226

Zhang X, Yazaki J, Sundaresan A, Cokus S, Chan SWL, Chen H, Henderson IR, Shinn P, Pellegrini M, Jacobsen SE, et al. 2006. Genome-wide high-resolution mapping and functional analysis of DNA methylation in *Arabidopsis*. *Cell* **126:** 1189–1201. doi:10.1016/j.cell.2006.08.003

Zhang Y, Liu T, Meyer CA, Eeckhoute J, Johnson DS, Bernstein BE, Nusbaum C, Myers RM, Brown M, Li W, et al. 2008. Model-based Analysis of ChIP-Seq (MACS). *Genome Biol* **9:** R137. doi:10.1186/gb-2008-9-9-r137

Zhang X, Bernatavichute YV, Cokus S, Pellegrini M, Jacobsen SE. 2009. Genome-wide analysis of mono-, di- and trimethylation of histone H3 lysine 4 in *Arabidopsis thaliana*. *Genome Biol* **10:** R62. doi:10.1186/gb-2009-10-6-r62

Zhang W, Friebe B, Gill BS, Jiang J. 2010. Centromere inactivation and epigenetic modifications of a plant chromosome with three functional centromeres. *Chromosoma* **119:** 553–563. doi:10.1007/s00412-010-0278-5

Zhang X, Singh J, Li D, Qu F. 2012. Temperature-dependent survival of *Turnip crinkle virus*-infected *Arabidopsis* plants relies on an RNA silencing-based defense that requires DCL2, AGO2, and HEN1. *J Virol* **86:** 6847–6854. doi:10.1128/JVI.00497-12

Zhang R-G, Li G-Y, Wang X-L, Dainat J, Wang Z-X, Ou S, Ma Y. 2022. TEsorter: an accurate and fast method to classify LTR-retrotransposons in plant genomes. *Hortic Res* **9:** uhac017. doi:10.1093/hr/uhac017

Zhang J, Yuan J, Lin J, Chen L, You L-Y, Chen S, Peng L, Wang C-H, Du J, Duan C-G. 2023. Molecular basis of locus-specific H3K9 methylation catalyzed by SUVH6 in plants. *Proc Natl Acad Sci* **120:** e2211155120. doi:10.1073/pnas.2211155120

Zhong X, Hale CJ, Law JA, Johnson LM, Feng S, Tu A, Jacobsen SE. 2012. DDR complex facilitates global association of RNA polymerase V to promoters and evolutionarily young transposons. *Nat Struct Mol Biol* **19:** 870–875. doi:10.1038/nsmb.2354

Zhong X, Hale CJ, Nguyen M, Ausin I, Groth M, Hetzel J, Vashisht AA, Henderson IR, Wohlschlegel JA, Jacobsen SE. 2015. DOMAINS REARRANGED METHYLTRANSFERASE3 controls DNA methylation and regulates RNA polymerase V transcript abundance in *Arabidopsis*. *Proc Natl Acad Sci* **112:** 911–916. doi:10.1073/pnas.1423603112

Zhou M, Palanca AMS, Law JA. 2018. Locus-specific control of the de novo DNA methylation pathway in *Arabidopsis* by the CLASSY family. *Nat Genet* **50:** 865–873. doi:10.1038/s41588-018-0115-y

Zhou M, Coruh C, Xu G, Martins LM, Bourbousse C, Lambolez A, Law JA. 2022. The CLASSY family controls tissue-specific DNA methylation patterns in *Arabidopsis*. *Nat Commun* **13:** 244. doi:10.1038/s41467-021-27690-x

Ziegler P, Adelmann K, Zimmer S, Schmidt C, Appenroth K-J. 2015. Relative in vitro growth rates of duckweeds (Lemnaceae): the most rapidly growing higher plants. *Plant Biol* **17:** 33–41.

Zimin AV, Salzberg SL. 2020. The genome polishing tool POLCA makes fast and accurate corrections in genome assemblies. *PLoS Comput Biol* **16:** e1007981. doi:10.1371/journal.pcbi.1007981

Zimin AV, Marçais G, Puiu D, Roberts M, Salzberg SL, Yorke JA. 2013. The MaSuRCA genome assembler. *Bioinformatics* **29:** 2669–2677. doi:10.1093/bioinformatics/btt476

Zong J, Yao X, Yin J, Zhang D, Ma H. 2009. Evolution of the RNA-dependent RNA polymerase (RdRP) genes: duplications and possible losses before and after the divergence of major eukaryotic groups. *Gene* **447:** 29–39. doi:10.1016/j.gene.2009.07.004

Received April 30, 2024; accepted in revised form February 6, 2025.